

## Imaging Plant Cells

Nuno Moreno, Susan Bougourd, Jim Haseloff, and José A. Feijó

### INTRODUCTION

The history of imaging plant cells is intimately related to the very development of microscopes and microscopical techniques. Some of the early microscopists made extensive use of plant specimens, and Hooke's description of cork microstructure (Fig. 44.1) will stand in the imagination of many as the structural foundation for cell theory. There are several reasons for this to have happened: in many respects plant tissues are easier to deal with, easier to slice and peel to the necessary thickness for observation, they have more water, and consequently are less optically dense than many other tissues, often they are naturally pigmented and the cells are usually larger. Above all, the existence of a skeletal cell wall composed of cellulose and other molecules makes plant cells extraordinarily geometric and highly regulated in their structural features. In many instances, these structural components of the plant cell form the basis of its function, making microscopical analysis a recurrent method for cell and developmental biology research.

Since the 17th century, many gifted microscopists have made cumulative accounts of the different levels of plant cell structure. Perhaps the first truly specialized plant microscopist was Grew (1673), who initiated the first systematic study of plant micro-anatomy. Robert Brown, Amici, Schleiden, and Nawaschin are among the many notables who contributed to the description of some of the fundamental biological features of plants, such as their reproductive cycles, mostly using microscopes as tools. More recently, the seminal textbooks of Esau (1977a,b) and Fahn (1990) systematized definitively the histological and cellular features of higher plants. Plant cell ultrastructure has subsequently been described and systematized in detail in many textbooks and atlases, such as the ones produced by Gunning and Steer (1996). This effort was recently complemented by an extensive review on CD-ROM that stands, and probably will stand for a long time, as a central reference for anyone seeking information on microscopical data concerning plant cells (Gunning, 2003; <http://www.plantcellbiologyoncd.com>).

The developments in technology and reagents that brought fluorescence-based methods to microscopy have also become prevalent in plant cell biology (Lloyd, 1987). However, plant cells do present a challenge to fluorescence microscopy because they often contain pigments and complex excitable molecules in subcellular structures that generate copious autofluorescence. In many circumstances this is a nuisance in terms of signal-to-noise ratio: the autofluorescence can swamp signal from other fluorescent probes

being studied. Furthermore, without the optical sectioning of the confocal microscope, autofluorescence glaring from all planes may obscure the signal from any in-focus structural information. Naturally, confocal imaging has made a strong impact in the area of plant-cell imaging. All these problems have been addressed in large and excellent reviews about applications of confocal microscopy to plant cell biology (Hepler and Gunning, 1998), imaging ions and other advanced methods (Blancaflor and Gilroy, 2000), and hand- and textbooks on methods and applications (Galbraith *et al.*, 1995; Hawes and Satiat-Jeunemaitre, 2001).

Green fluorescent protein (GFP) and other genetically-encoded fluorescent probes have made a substantial impact on the field (Haseloff and Amos, 1995; Haseloff *et al.* 1997), and extensive lists of references of different applications, spectral conditions, and transient expression systems are available (Brandizzi *et al.* 2002). Detailed comparisons of the relative merits between conventional and widefield (Shaw, 2001) and between two-photon excitation and confocal (Feijó and Moreno, 2004) have shown that there are specific niches for all methods, and probably none should be considered universal, irrespective of their price and sophistication. Previous reviews also included detailed protocols for image acquisition using these different methods. A very useful collection of practical criteria for probe choice, empirical methods, and many tricks for immobilization, perfusion, and loading protocols are described by Fricker and colleagues (2001).

Specific methods for some of the most-used cell and tissue types have also been described (e.g., Kodama and Komamine, 1995; Raghavan, 1995; Sheen, 1995). Various fixation and other histological methods specific for plant cells are extensively described in many references (e.g., Spence, 2001), including complex and sophisticated freeze-fixation and freeze-substitution methods (Galway *et al.*, 1995; Parthasarathy, 1995).

However, recent years have been marked by the introduction of less invasive methods and vital probes, with a strong emphasis on those that are genetically encoded. The focus now is on keeping cells and tissues intact and alive, and this offers the added value of enabling one to study the true dynamics of vital processes. Vesicle trafficking (Bolte *et al.*, 2004), individual gene expression (Shav-tal *et al.*, 2004), and cytoplasmic streaming dynamics (Shimen and Yokota, 2004) are just a few examples of the living processes now reachable using state-of-the-art microscopy in combination with genetic and molecular techniques. We will thus focus this chapter on recent developments that might impact plant biological research beyond the topics covered in the earlier reviews.

Nuno Moreno • Instituto Gulbenkian de Ciência, PT-2780-156 Oeiras, Portugal

Susan Bougourd • University of York, York YO10 5DD, United Kingdom

Jim Haseloff • University of Cambridge, Cambridge CB2 3EA, United Kingdom

José A. Feijó • Instituto Gulbenkian de Ciência, PT-2780-156 Oeiras, Portugal, and Universidade de Lisboa, PT-1749-016 Lisboa, Portugal

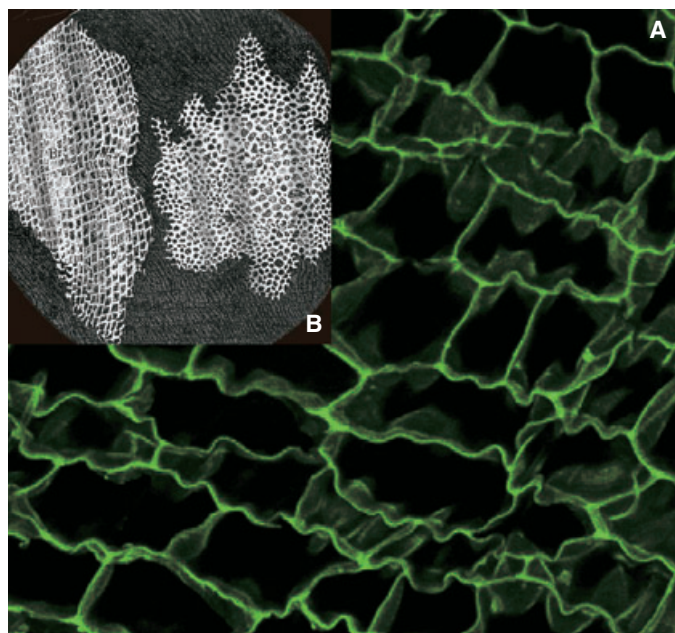


**FIGURE 44.1.** (A) Cork now and then! Comparison of Robert Hooke's picture (B) and state-of-the-art laser-scanning microscopy (A) of a cork slice, having a time difference of almost 350 years. It was in the book *Micrographia* published in 1665 that Hooke used the term "cells" for the first time to describe the element of this regularity. Despite the obvious differences (one drawn by hand, the other based on digital acquisition of optical slices and software enhancement by using maximum-intensity projection), the evidence of the highly regular structure of plant cells is early evident in Hooke's image, and underlies the close relationship between form and function in plant cells. However, the confocal image also shows one of the most prevalent features of plant cells: the almost ubiquitous existence of autofluorescence in various sub-cellular structures, a factor that can be both informative and a problem to deal with when imaging probes with overlapping fluorescence spectra.

## THE EVER PRESENT PROBLEM OF AUTOFLUORESCENCE

Light is potentially damaging to cells, yet plants live in the fast lane. In order for photosynthesis to proceed, leaves and other aerial parts are often exposed to high levels of light radiation, and evolution has resulted in a number of mechanisms for filtering photons before they reach sensitive parts inside the cell. In addition, many plant cell walls accumulate complex hydrophobic molecules that regulate apoplastic water loss and movement (e.g., suberin in cork; Fig. 44.1), and a plethora of secondary metabolites, many working as pigments, have evolved for ecological or allelopathic reasons. Many of these molecules use varied pathways to dissipate photo-excitation, namely non-radiative decay or relaxation, energy transfer, photosynthesis, and fluorescence. Unfortunately, the latter is common and autofluorescence is a natural feature of almost every plant cell (see Chapter 21, *this volume*, for detailed spectra).

This autofluorescence is a nightmare for many fluorescence applications. On fixed, sectioned, and stained specimens, protocols using strong oxidizing agents such as chlorine bleach, chloral hydrate, or sodium-borohydride have long been used to reduce autofluorescence (Shaw, 2001; Chapter 18, *this volume*). Efficient as they are, these techniques cannot be used when imaging living cells, and the molecular degradation they produce can even destroy the specificity of immunostaining. Many fixation reagents, such as glutaraldehyde, also add to the problem by generating autofluo-

rescent Schiff bases and delocalized electron resonance transfer when they react with cellular components.

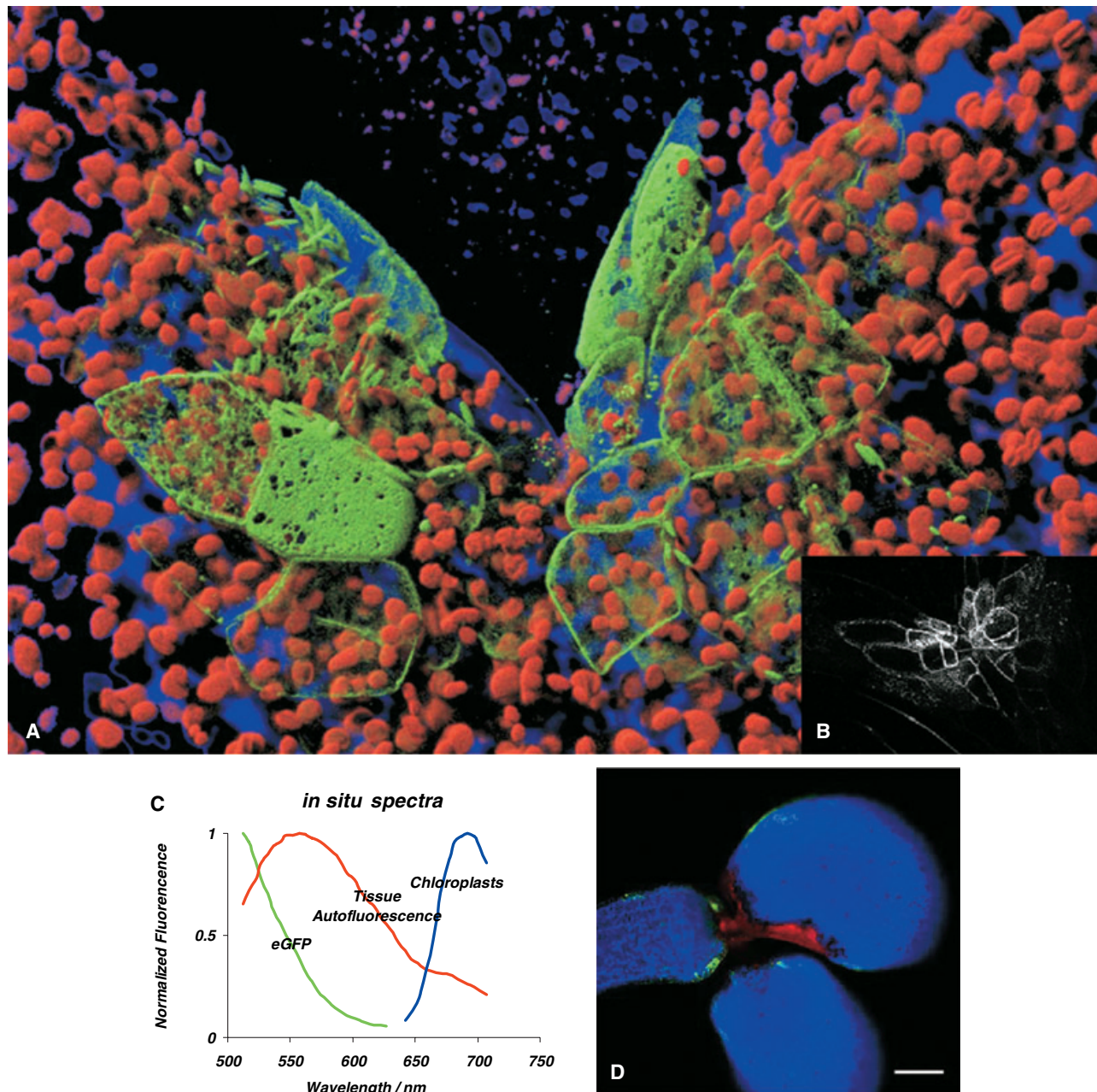
The problem is illustrated in Figures 44.1 and 44.2. In Figure 44.1(A), the same cork that Hooke could describe because of its opacity to photon transmission is also shown by state-of-the-art confocal microscopy because the walls of dead cells are impregnated with suberin, a complex lipid with strong autofluorescence. As the cells are empty, after extended focus stacking, the cell walls can be seen with great detail and the confocal capacity of rejecting out-of-focus light renders images with great visual depth.

Figure 44.2 shows what is probably the most common source of imaging problems: the green tissues. Chlorophyll accumulates inside plastids that occur in great numbers in green tissue (the round red organelles in this image). Although in the shoot meristem region, depicted in Figure 44.2, the cell wall is still relatively immature and thus has less autofluorescence (shown in blue), these two signals render the observation of other fluorophores (in this case GFP in the endoplasmic reticulum (ER), shown in green) almost impossible unless the out-of-focus light can be rejected and strong spectral separation is available.

Cell wall autofluorescence swamps the signal from added probes and the absorption and scattering of both the excitation and the signal severely limits the distance that one can image into the tissue. The common way of dealing with spectral mixing is to use selective dichroic/emission filters, with the excitation peak as narrow as sensitivity allows. In a relatively young organ such as that shown in Figure 44.2, good results are obtainable with standard confocal settings (in this case, using a Zeiss Pascal). The importance of being able to produce stringent optical sections is illustrated in Figure 44.2(B), which shows a two-photon image of the GFP in the central section of the same plantlet. The image is almost clean of the other sources of signal.

On a more physical basis, absorption in green tissues usually involves both excitation of a first excited singlet state (responsible for red absorption) and excitation of a second excited singlet state (responsible for blue absorption). In both cases, emission is mainly in the near-infrared because the blue-excited state relaxes to the first singlet [Malkin and Niyogi 2001; Figure 44.2(C)]. This complex response can be either a drawback or a bonus. Chloroplasts emit farther into the red [Fig. 44.2(D) in false blue], but other emissions in the visible spectrum can superimpose important information. Overall, they usually have a broad emission spectrum, and it is not a trivial matter to discriminate it from labeling, even in a spectral microscope.

Many recent confocal microscopes come equipped with the capacity for spectral analysis, and this facility is becoming a useful tool for discriminating against autofluorescence. There are two ways of using the new spectral tools. In the first, one is only concerned with the emission from a single dye, and chooses the narrowest, most selective emission window for the dye involved. This is a one-step method, and only a single reference spectrum is needed for each series of observations. In the second method, one uses linear spectral unmixing to separate the emission of different dyes. Although speed is usually not an issue with the first method, it may be with the second, especially if the signal in the different channels must be acquired sequentially. However, parallel acquisition often implies channels only 10 nm wide and when an already weak signal is distributed among several narrow spectral windows, there is even less signal in each one. As a result, low signal level can be a problem and no commercial system is devoid of limitations in that respect. Although low signal can be overcome to some extent by more laser power, this can lead to other sorts of physical limitations, particularly singlet-state saturation of the dye and photodamage to the specimen.



**FIGURE 44.2.** Three-dimensional reconstruction of an *Arabidopsis* hypocotyl/cotyledon done using a Zeiss Pascal with three emission channels and three laser lines (405, 488, and 633 nm) using a 63× Plan Apochromat NA 1.4 oil-immersion objective. This is an enhancer trap line with GFP linked to an ER domain protein, which in this case was activated on the meristematic primordial cells. Using the normal dichroic/emission filters, GFP (green) is well resolved from the chloroplasts (red) because their emission shows up mainly in the near infrared. The immature (thus dimmer in terms of autofluorescence) cell wall appears as shown in false blue. Insert (B) shows a different way of resolving the GFP signal, by two-photon excitation (TPE) at 870 nm. Because the excitation wavelength is not as optimal for the chlorophyll as it is for GFP, the red plastids seen in (A) are much dimmer or invisible. (C) *Arabidopsis* seedling spectra traced *in situ* with a Leica SP2 AOBS. After making a lambda scan from 500 to 700 nm with a spectral gate width of 30 nm, using a 488 laser line and a 10× Plan Apochromat NA 0.4, a spectrum from each part of the tissue was traced for eGFP, cell wall and chloroplasts autofluorescence. With these emission spectra it becomes possible to unmix the lambda-stack (D). This software tool comes with all the spectral confocal systems (Leica SP2 AOBS and Zeiss 510 Meta) and works in a similar way to spatial deconvolution but in this case the bleed-through is not caused by out-of-focus signal, but from overlapping fluorescence emission. Bar = 200 μm.

Figure 44.2 shows an *Arabidopsis* seedling with GFP expression in the ER. Reference spectra were generated for the different pigments [Figure 44.2(C)] and the respective signals extracted from the raw xyzλ-image data (a so-called lambda stack), and then merged again with false colors [Fig. 44.2(D)]. It is clear that the channels have been sharply separated. While the principle works, there are limitations, and when several fluorescent proteins are

present, it can be more difficult to separate colors, especially if more than one of them occurs in the same voxel. In any case, one needs a specimen capable of producing lots of signal.

As usual there are several engineering solutions to the problem of spectral detection. Leica uses a prism and a set of moveable mirrors to break the spectrum of emitted light into three or four segments, each going to a separate photomultiplier tube (PMT).

Zeiss uses a grating to disperse the emission spectrum over an array of 32 mini-PMTs, and has facilities to digitize as many as 8 channels from any combination of the 32 outputs (Nikon and Olympus are also launching their own solutions). There are pros and cons to each method: generally speaking one can say that the latter gain in terms of temporal resolution during live imaging, but perhaps at the cost of some sensitivity, especially in the red extreme of the spectrum.

Once the spectral data have been obtained, they must be deconvolved (or unmixed) using programs similar to those used to deconvolve widefield structural data (see Chapters 23, 24, and 25, *this volume*), except that, instead of starting with a point-spread function, one starts with stored spectra of each of the dyes present. Least-squares algorithms are used to fit the spectral data measured in each voxel or region to a linear sum of the spectra of the dyes expected to be present. As all the light used by the spectral detector comes through a single pinhole, one cannot use pinhole size to balance the signal intensities from different dyes. Consequently, the procedure works best when the signals from all the various dyes are approximately equal in strength.

## SINGLE-PHOTON CONFOCAL MICROSCOPY

Because plant tissue generally consists of deep layers of highly refractile cell walls and aqueous cytosol and contains various auto-fluorescent and light-scattering components, intact tissue proves a difficult subject for fluorescence microscopy. However, direct imaging of living tissue is possible using suitably-corrected microscope optics. Plant seedlings or excised tissues can simply be mounted in water for microscopy and examined using a long-working-distance water-immersion objective to minimize the effects of spherical aberration when focusing deep into an aqueous sample. Even with the use of such specialized objectives, using single-photon excitation image quality degrades rapidly for optical sections deeper than 60 to 80  $\mu\text{M}$  within the tissue. However, the small size of seedlings, such as those of the model plant *Arabidopsis thaliana*, allows very useful imaging despite this limitation. For example, median longitudinal optical sections can be obtained from intact roots. This direct approach to imaging plant materials has been reviewed elsewhere (Haseloff, 2003).

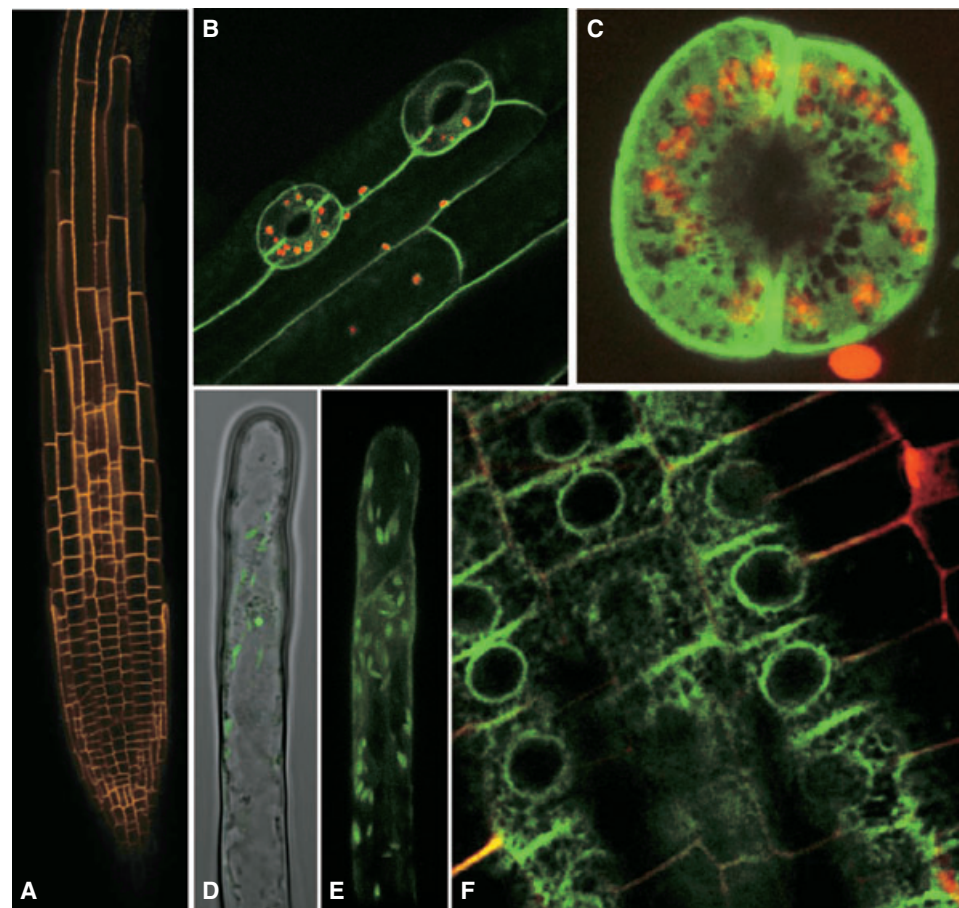


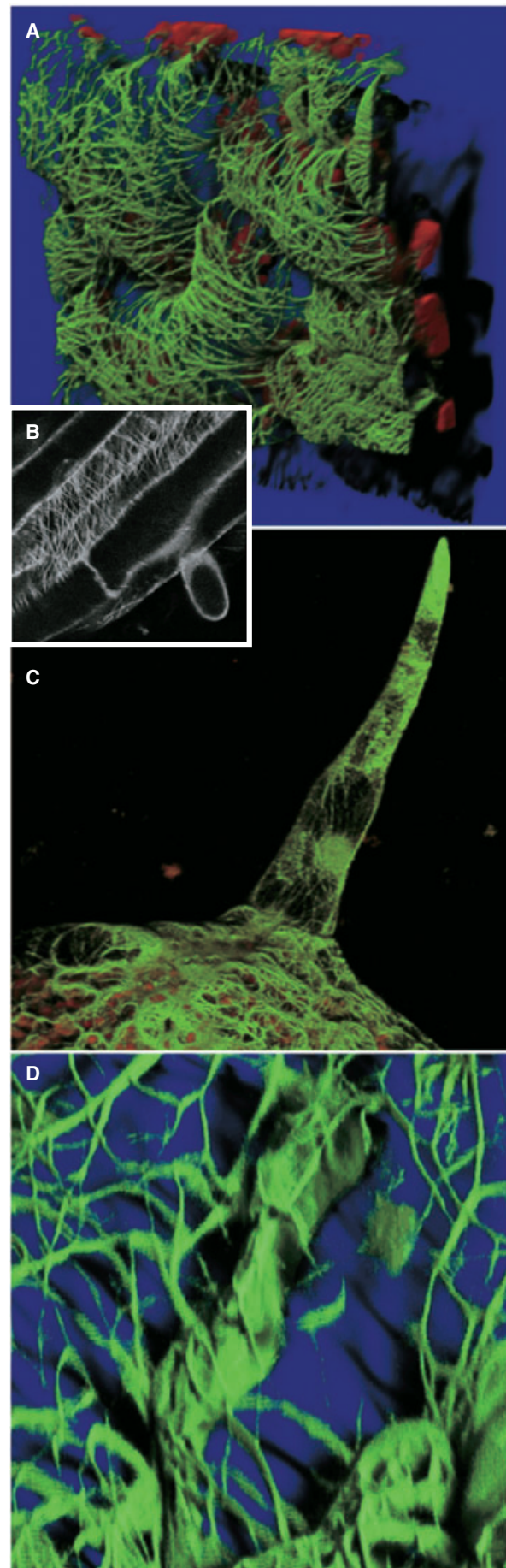
**FIGURE 44.3.** (A) Optical section of an *Arabidopsis* root with a random insertion (Cutler *et al.*, 2000) of Clontech-YFP targeted to the plasma membrane (confocal image excited at 525 nm using a Leica SP2 AOBS). (B) Seedling shoot epidermis from a line similar to that shown in (A), but with the Clontech-GFP imaged with TPE at 930 nm. Despite the non-optimal optical response to this wavelength, the beam has enough power to produce the desired excitation and yields outstanding results in terms of tissue penetration and signal-to-noise ratio. (C) Dual-emission confocal imaging from a stoma in which the ER is stained with mGFP5 (enhancer trap line) and the chloroplasts are emitting auto-fluorescence. Mixed widefield and fluorescence (D) and confocal fluorescence (E) of mGFP5 enhancer-trap transformed *Arabidopsis* root hair. GFP is fused to an ER motif, and the dynamics of the big ER inclusions are clearly visible. (F) Double-emission of ER-targeted mGFP5 (Siemering *et al.*, 1996) fusion product with the SCARECROW gene (Wysocka-Diller *et al.*, 2000). Despite the low expression level, the ER and nuclear envelope are clearly resolved in the endodermis, four cell layers deep into the root. The cell wall is stained with vital PI. The optical-sectioning properties of TPE are well illustrated in the sharp fading pattern of the cell wall tangential section.

**FIGURE 44.4.** Leaf epidermal cell of a transgenic *Arabidopsis* with a microtubule-associated protein (MAP4) GFP fusion, imaged with a Zeiss Pascal confocal. z-stacks were acquired (B) and 3D volume-rendered. Red organelles are plastids. The subcortical distribution of the microtubules is clearly visible due to the depth created by the rendering algorithm. This construct, while producing excellent results for epidermal microtubules, seems useless for labeling microtubules in other cells. (C, D) Leaf trichome of a transgenic *Arabidopsis* with the actin-bundling protein talin fused with GFP, imaged with a Zeiss Pascal confocal and processed as in (A). Amplification in (D) is particularly noticeable by the details of the actin bundles inside these cells. However, great care must be used in interpreting this result, because under a constitutive strong promoter, talin is prone to creating “artificial” cables of actin, which are not supported by other means of visualization (Ketelaar *et al.*, 2004).

Direct visualization of GFP fluorescence in living tissues is not prone to fixation or staining artifacts, and can provide images of exceptional clarity. Moreover, the activities of living cells, such as cytoplasmic streaming, are clearly evident during microscopy. Ordinarily, movement within a sample is a nuisance, placing constraints on the use of sometimes protracted techniques for noise reduction during confocal microscopy, such as frame averaging. However, it is also possible to monitor dynamic events by time-lapse confocal microscopy, and this combination of a vital fluorescent reporter with high-resolution optical techniques has proven valuable in cell biological and physiological experiments. We have also found that autofluorescent chloroplasts, normally present in the upper parts of the plant, and certain red fluorescent dyes can provide useful counter fluor for GFP. For example, propidium iodide can be applied to live seedlings in water, to specifically label root cell walls, and allow accurate identification of GFP expressing cells [Fig. 44.3(F)].

It is now possible to genetically mark cells or subcellular compartments within a living organism using GFP and to visualize these directly during development. A number of collections of transgenic lines have been developed where GFP gene expression has been targeted to particular cell types or where GFP protein fusions have been used to decorate cell compartments in *Arabidopsis*. For example, Cutler and colleagues (2000) have produced a library of transgenic *Arabidopsis* lines that express random cDNA-GFP fusions. The fluorescent protein is targeted to various subcellular compartments in these lines, and they provide a useful source of dynamic markers for nuclei, plastids, different membranes, and other compartments [Fig. 44.3(A,B)]. In addition, enhancer trap strategies have been used to direct the expression of a foreign transcription activator, GAL4, in different cell types in *Arabidopsis* (Haseloff, 1999a,b). The GAL4 gene was inserted into the *Arabidopsis* genome, using *Agrobacterium tumefaciens*-mediated transformation. Expression of the GAL4 gene is dependent upon the presence of adjacent genomic enhancer sequences, and so different patterns of expression were generated. The inserted DNA also contains a GAL4-responsive GFP gene, and patterns of GAL4 gene expression are immediately detectable, with each GAL4-expressing cell marked by green fluorescence. These lines provide a valuable set of markers, where particular cell types are tagged and can be visualized with unprecedented ease and clarity in living plants [Figs. 44.2 and 44.3(C–E)]. The collections of cDNA fusions and GAL4 enhancer trap lines are available through the *Arabidopsis* stock centers.

A particularly exciting field has also emerged with the successful development of GFP-fusion products with cytoskeleton associated proteins, which enable high resolution imaging of both microtubules (Fig. 44.4) and actin microfilaments



[Figs. 44.4(C,D)]; see also Chen *et al.*, (2003); and Shaw *et al.*, (2003). Use of over-expressing constructs of cytoskeleton binding proteins can, however, disrupt the delicate balance of the dynamic instability that usually takes place during the polymerization of the cytoskeleton under physiological conditions, as recently demonstrated for talin (Ketelaar *et al.*, 2004). Despite their obvious beauty and apparent information, these images and their spatial and temporal kinetics should be interpreted with great care.

### Staining Plant Tissues

As an alternative to direct imaging of live specimens, it is possible to fix and stain intact plant tissues and then to clear the material using a high-refractive-index mounting medium. It is then possible to obtain high-resolution optical sections from deep within intact tissues using objectives corrected for oil immersion.

A wide variety of staining techniques have been adopted for plant specimens over the last 150 years. Perhaps the most widely used general tissue stains are Safranin O and Haematoxylin. These are often accompanied by the use of counterstains such as Fast Green, Orange G, or Alcian Blue. In addition, there are a large variety of more specific staining techniques that have been developed for particular plant materials and organelles. For example, Feulgen staining has been used for specifically labeling DNA, the periodic acid–Schiff reaction can be used to label carbohydrates, Aniline Blue for labeling callose, Nile Red for oil bodies, and Phloroglucinol for lignin. A multitude of published protocols are available. An excellent, recently published source of procedures can be found in Ruzin (1999).

Interestingly, many of the synthetic dyes used for plant microtechnique are highly fluorescent. This is particularly so for the red, orange, and yellow dyes in the azine (e.g., Safranin O), acridine (e.g., Acridine Orange), and xanthene (e.g., Rhodamine) families. Thus, many classical histological techniques unintentionally produce specimens that are intensely fluorescent. In addition, aldehyde fixation, certain mountants, and long-term storage of stained preparations can result in tissue fluorescence, and the high concentration of stains deposited in the sections can lead to metachromasia (Mason, 2000). In our hands, it is rare to find stained and sectioned botanical material that is not highly fluorescent. Current confocal microscopes can sometimes allow the clean separation of different fluorescent emission signals and the balancing of signal levels in different channels. Thus, fluorescent images of exceptional clarity and vivid color can be easily obtained (Fig. 44.5). In addition, the optical sectioning properties of the confocal microscope can be used to collect clear images from within thick sections and whole mounts.

### Clearing Intact Plant Material

The three-dimensional (3D) anatomical arrangements of plant cells have conventionally been observed using microtomy techniques. However, the laborious nature of thin sectioning, the problem of obtaining the desired plane of section, and difficulty of obtaining a complete series of sections has limited its use to the skilled and patient. Optical sectioning has many advantages from the point of view of speed and simplicity, and it allows software reconstruction of whole mount specimens, assembled from a series of *z*-axis images. However, it is difficult to observe cellular details deep in living plant tissue. Any light penetrating the tissue must pass through many layers of cytoplasm, watery vacuoles, and highly refractile cell walls. The different refractive indices of the material contribute to spherical aberration, and particulate subcellular

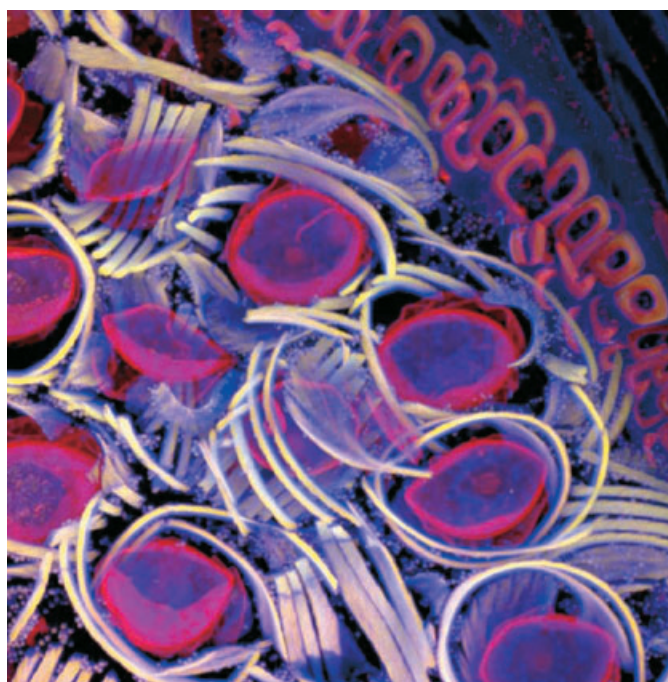
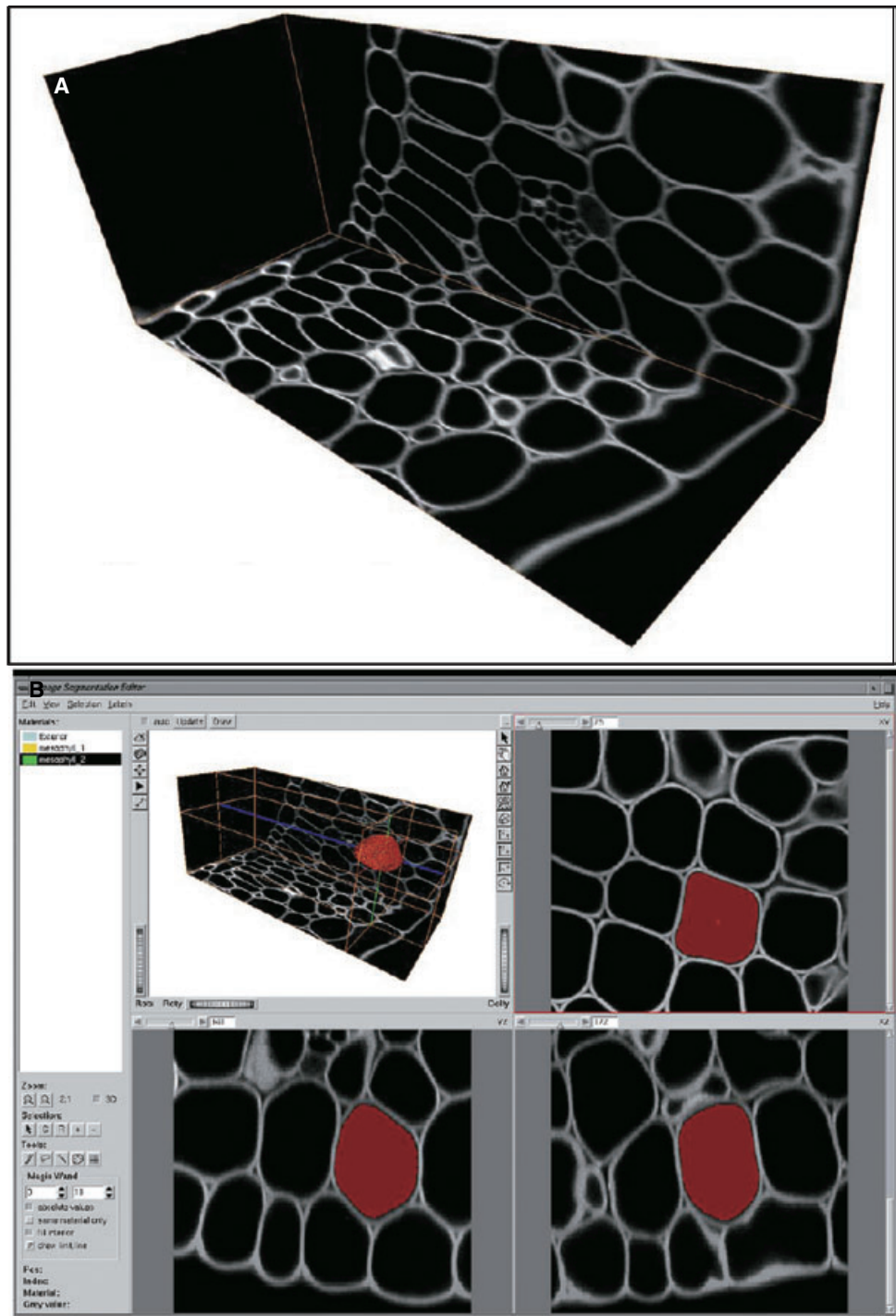


**FIGURE 44.5.** Confocal microscopy of *Equisetum arvense* spores. *Equisetum* sporangiophore tissue was fixed, cleared in xylene, embedded in paraffin, sectioned using a microtome, and stained with Safranin O and Fast Green FCF. A *z*-series of three-channel color images were collected using a Leica SP confocal microscope with laser excitation at 488 nm, 568 nm, and 633 nm. These were visualized using a maximum intensity projection algorithm. Spores can be seen within the sporangiophore. The spores are surrounded by exospore elaters, and lignified cells involved in sporangial dehiscence are seen (top right).

matter also causes light scattering. Various techniques have been developed in order to produce samples with glass-like optical properties and to maximize image quality. Clearing agents, such as xylene, clove oil, cedar oil, and chloral hydrate have been adopted and combined with compatible mountants such as Canada balsam and Hoyer's solution. All of these reagents have a high refractive index similar to that of glass (~1.55). As a result of these clearing treatments, tissue sections become more transparent, greatly reducing problems with light scattering and spherical aberration as long as oil-immersion lenses are used. This allows high-resolution imaging of thin sections. When the same techniques are applied to thick sections or whole mounts, the results of clearing are even more startling. However, the stain or fluorochrome is generally distributed throughout the cleared tissue and details deep in the sample are still obscured by overlying signal. Here the confocal laser-scanning microscope proves its worth. High-resolution optical sections can be collected to distances of greater than 200  $\mu\text{m}$  in such cleared samples. The depth of image collection is limited mainly by the working distance of available high-numerical-aperture objectives. The application of classical, highly fluorescent stains and clearing techniques creates a new field of opportunities for modern confocal microscopy and computerized display methods.

Recently, classical botanical methods have been modified to allow intense and specific staining of plant cells and clearing for 3D microscopy. For example, Aniline Blue has been used as a stain for the cell contents of *Arabidopsis* embryos subjected to 3D imaging (Bougourd *et al.*, 2000). More recently, plant carbohydrates have been labeled by treatment with periodic acid to

**FIGURE 44.6.** (A) Deep optical sectioning of cleared *Arabidopsis thaliana* root tissues. Mature *Arabidopsis* embryos were treated with periodic acid to produce aldehyde groups within carbohydrates, and stained using a pseudo-Schiff reaction to specifically label the cell walls. The tissues were mounted in a chloral-hydrate-based clearing agent for microscopy. The combination of clearing and intense staining allows deep optical sectioning of an entire embryo cotyledon. A series of 736 optical sections were obtained to span the cotyledon, producing a dataset with a depth of 147  $\mu\text{M}$ . (B) 3D segmentation of plant cells. A series of confocal optical sections, corresponding to a segment of cotyledon from an *Arabidopsis* embryo, is visualized using the AMIRA orthogonal slicing routines. The AMIRA 3D segmentation editor was used to seed and label particular voxels that correspond to chosen plant cells within the confocal dataset. The use of a specific cell wall stain allows easy selection of the internal volumes of individual cells. A closed, triangulated surface could then be formed over the selected group of voxels, using a marching-cubes algorithm. Rendered cells are displayed at the correct position and scale within the dataset, to build an accurate representation of the shapes, arrangement, and connectivity of cells within the tissue.



produce aldehyde groups that are reacted with fluorescent pseudo-Schiff reagents. If fixed plant tissue is treated in this way, cell walls (and starch-containing plastids, if present) become intensely and covalently labeled with the fluorophore. The labeling of wall material produces a complete outline of each cell. The tissue can then be directly cleared in a high-refractive-index agent containing chloral hydrate, and mounted in Hoyer's solution for microscopy [Haseloff and Bougourd, unpublished results; Fig. 44.6(A)]. The combination of high levels of fluorescence and high refractive index mountant allows the collection of extended  $z$ -series images at very fine resolution (0.1–0.5  $\mu\text{M}$  steps), using a confocal aperture close to 1 Airy unit, and without fear of photobleaching or

signal and resolution loss due to spherical aberration. Imaging to a depth of around 200  $\mu\text{m}$  allows simple optical sectioning throughout an entire *Arabidopsis* root at high resolution. In fact, every cell within a mature *Arabidopsis* embryo can be clearly visualized (Fig. 44.6).

### 3D Reconstruction

The basic features of a plant's body plan are established during embryogenesis, but its final form results from the continued growth of meristems and the formation of organs throughout its life, often in a modular and indeterminate fashion. Because plant

cells are constrained by rigid cell walls and are generally non-motile, there is the clear possibility that cell fates within a meristem are determined by lineage. However, evidence from plant chimera and wounding studies have demonstrated a more important role for cell–cell interactions during fate determination. It is likely that, during plant development, positional information is exchanged between cells, and that the fate of cells within a developing tissue is determined by a network of local cellular interactions. In order to dissect such a network, it is crucial that we can clearly map individual cells and their neighbors inside intact meristems — and have means to manipulate them. Thus, the cellular anatomy of plants is of particular relevance to the understanding of development and morphogenesis.

Three-dimensional visualization techniques similar to those used in medical imaging can be applied to confocal datasets. This involves the selection and labeling of particular voxels that correspond to a 3D object of interest. Various techniques are available for selecting volumetric objects, which range from the fully manual to automatic tools that detect volume boundaries through differences in local intensity or texture (see Chapters 14 and 15, *this volume*). The use of specific staining techniques can aid the labeling process. For example, cell wall staining produces an outline of every cell in the tissue. This is very helpful as it allows the use of automatic segmentation tools to determine the interior volume of a chosen cell. We routinely use AMIRA, a general-purpose physical modeling and data visualization program (Mercury Computer Systems, [www.tgs.com](http://www.tgs.com)), for our 3D visualization and segmentation [Fig. 44.6(B)]. The software provides an interface for visualizing large multi-dimensional confocal

microscopy datasets. Amira provides a very useful set of input/output, data handling and visualization modules, and allows software routines to be combined in a modular fashion. This allows specialized 3D reconstruction and visualization techniques to be applied in a flexible way to different types of data, including confocal datasets. In addition, a developer's version, AMIRADev, allows the incorporation of custom visualization techniques. The program provides a simple interface, sophisticated, fast visualization routines, is affordable and robust, and is suitable for both high-end PC and UNIX hardware.

### 3D Segmentation

High-resolution confocal datasets can be rapidly segmented to allow direct visualization of cell arrangements within intact plant embryos and meristems. The large data files, up to 250 MB in size, can be directly rendered to allow excavation of the data, production of sections in arbitrary planes, and rendering of surface features. In practice, cells are generally chosen by placing a “seed point” manually within the center of a cell in the confocal dataset. This seed is then inflated in three dimensions to find the cell boundaries that are marked by a high staining intensity (Fig. 44.7). The program provides a segmentation editor for this purpose [Fig. 44.6(B)]. The exterior geometry of a segmented cell can then be described using a “marching cubes” algorithm, which if needed can be converted to a solid geometry for the computer-assisted milling of 3D models or for finite element analysis [Fig 44.8]. We can now routinely reconstruct the cellular structure of entire meristems for various experiments.

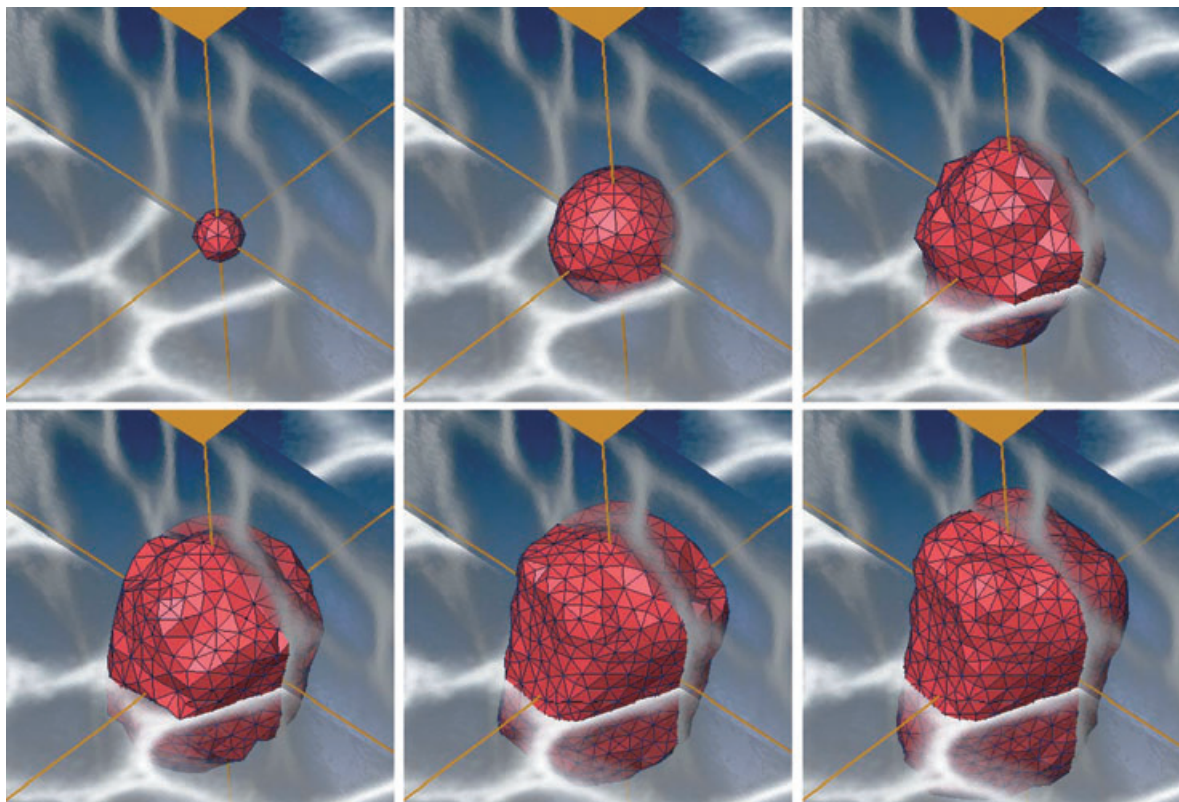
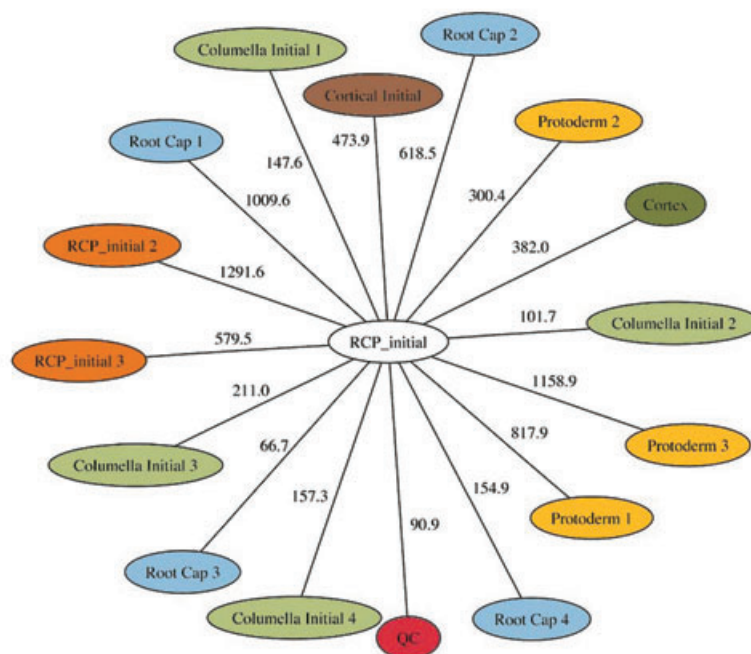
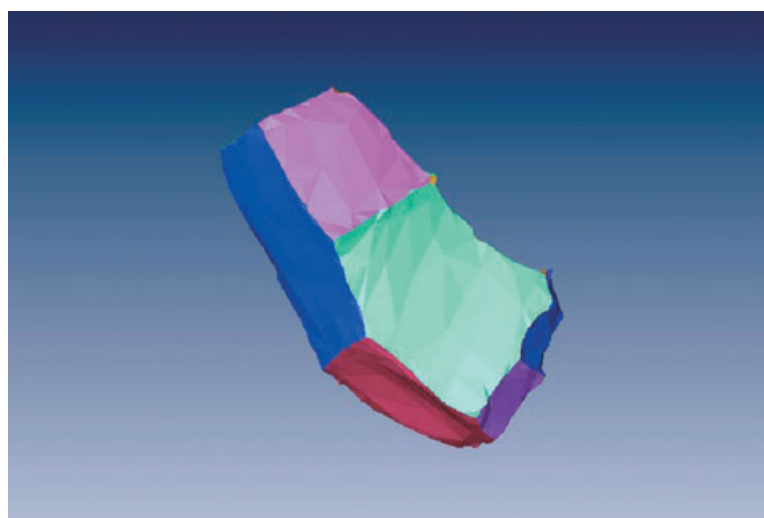


**FIGURE 44.7.** Balloon model-based segmentation of plant cells. A deformable-mesh algorithm for segmentation was implemented in C++ as a software module inside AMIRA. The module allowed the interactive placement of a seed mesh within the dataset (top left panel). The surface was then inflated using a discrete-time physical model. Expansion was accompanied by adaptive subdivision of the surface during inflation, and ultimately was constrained by a “force” based on the image intensity gradient vector. Vertices on the surface are attracted to intensity maxima in the data, which correspond to the stained boundaries of the cell.

**FIGURE 44.8.** (A) Watershed algorithm for segmentation. Code from the National Library of Medicine Insight Toolkit ([www.itk.org](http://www.itk.org)) was adapted to provide a watershed algorithm for the AMIRA visualization platform. The algorithm was applied to a 3D dataset derived from the root primordium of an *Arabidopsis thaliana* embryo. A single, root-cap protodermal initial cell from the segmented dataset is displayed, and its different shared walls are shown color-coded. Each colored segment corresponds to a connection with a different neighboring cell within the meristem. (B) Graph of 3D connections between cells. Using the dataset shown in (A), an adjacency network was computed and cell–cell contact measured. This data was represented using graph-generation software (AT&T Graphvis). The 16 cells making contact with the root cap–protodermal initial (RCP\_initial) are shown on the diagram, with measurements of the area of each cell–cell contact.



There are many opportunities for improved analysis of this kind of 3D datasets. For example, plant cells are generally convex and simple in shape, and this allows the use of a more robust model-based segmentation approaches: a deformable mesh can be placed within a 3D dataset at chosen seed points and inflated (McInerney and Terzopoulos, 1996). The mesh simulates an elastic surface expanding from the interior of a cell. The surface evolves through a discrete-time physical model and adaptively subdivides to fit the object boundary (Fig. 44.7; Rudge and Haseloff, unpublished results). This type of model-based segmentation is much less sensitive to noise in the experimental data and produces a compact description of plant cell shapes directly. Other techniques produce an intermediate segmented volume, from which a surface must be generated and smoothed.

In addition, it is possible to automatically obtain a measurement of the number and area of shared walls between cells and their neighbors. These values are highly relevant biologically as they correspond to shared walls that contain plasmodesmata,

provide conduits for informational molecules that regulate cell behavior, and are an important parameter for modeling approaches. The watershed algorithm is based on the metaphor of water catchment basins in a landscape. First, an initial classification of all points into catchment-basin regions is done by tracing each point down its path of steepest descent to a local minima. The confocal image intensity is used as the landscape height. This process gives ridges between cells and shows slightly uneven terrain in the cell interiors. Next, neighboring regions and the boundaries between them are analyzed according to minimum-boundary height to produce a tree of merges among adjacent regions. By changing the “flood level,” we can interactively traverse the merge tree and thus finely tune the segmentation. The technique produces a single boundary between cells with no empty, unclassified intervening space. We can use this property to compute an adjacency network for the cells and measure cell–cell contact areas. This can then be represented diagrammatically using graph-generation software (Fig. 44.8; Rudge and Haseloff, unpublished results).

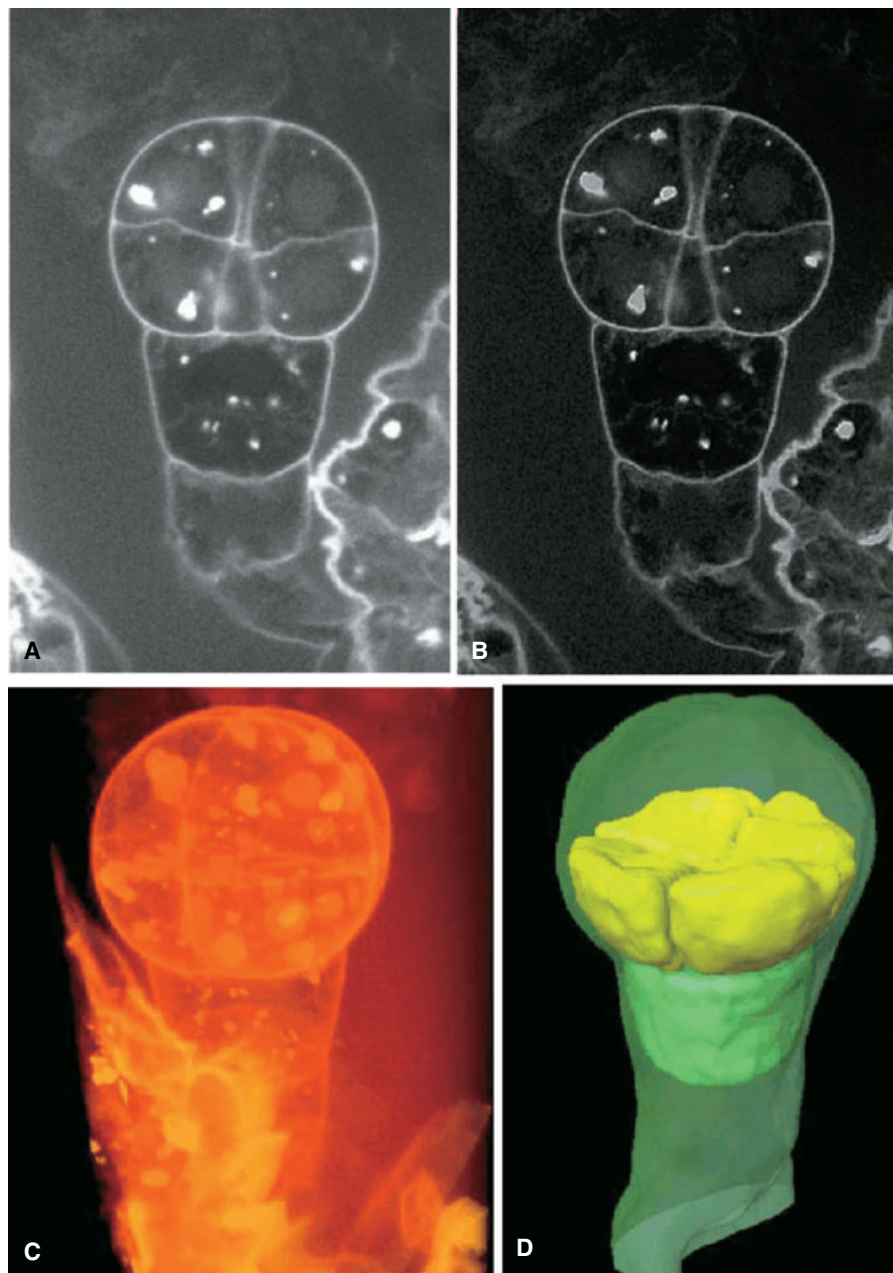


**FIGURE 44.9.** Three-dimensional reconstruction of cell arrangements within an *Arabidopsis thaliana* embryo. (A) An 8-cell *Arabidopsis* embryo was treated with periodic acid and stained, using propidium iodide as a pseudo-Schiff reagent. The sample was cleared with chloral hydrate and mounted in Hoyer's Solution. A z-series of confocal optical sections was collected, and a single optical section from near the middle of the 3D dataset is shown. (B) The 3D image was then processed using a deconvolution algorithm (Huygens Essential, Scientific Volume Imaging). A single optical section is shown from the processed volume. Deconvolution results in improved image detail and S/N. (C) Visualization of the deconvolved 3D dataset, using the Voltex module in AMIRA, provides direct volume rendering. The stalk-like embryo and some surrounding maternal tissues can be seen. (D) Cells in the lower-tier of the embryo (yellow) and upper cell of the suspensor (green) have been segmented, converted to new geometrical surfaces, and visualized within the dataset. The cells are shown within a semi-transparent outline of the embryo. Extracted cell geometries can be used to define regions of interest, or co-visualized with the original microscopy data.

These computer visualization methods, which are adapted from the medical imaging field, reduce large data sets to a much more compact and simple description of the 3D shapes and relative arrangement of cells in a meristem or embryo (Fig. 44.9). Because cell–cell signaling plays such an important role in plant development, these techniques show much promise for the analysis of genetically-perturbed plants, and as a basis for modeling the cellular interactions themselves.

### TWO-PHOTON EXCITATION: ARE TWO BETTER THAN ONE?

Recently, two-photon excitation (TPE) fluorescence microscopy has become a common tool in many advanced cell biology laboratories. A growing body of literature points to several advantages of TPE over other fluorescence imaging methods, with improved

signal-to-noise ratios, deep penetration, and benefits for living-cell imaging (Feijó and Moreno, 2004). TPE microscopy is still in an early stage of development and reproducible protocols, probes, and applications remain relatively scarce. However, botanical techniques already in use provide clear advantages. In particular, TPE is relatively immune to the presence of out-of-focus absorbing structures. This section covers some of the aspects of imaging plant cells using TPE.

### Improved Signal-to-Noise Ratio and Dynamic Range

Of all the possible advantages of TPE microscopy, the one we feel most confident to stress is the high signal-to-noise ratio (S/N) and dynamic range of the final signal. Generally speaking, once conditions have been sufficiently optimized to produce a good image, TPE provides better contrast, crispness, and image quality. Numer-

ous examples of this rule have been shown elsewhere (Feijó and Moreno, 2004, and references therein; see also Chapter 21, *this volume*). Comparison of images collected using single- and two-photon excitation showed much better detail and signal-to-noise ratio for the TPE data, especially for tangential sections at the extremes of a deep  $z$ -stack. On such sections, TPE resolves without loss of dynamic range, whereas confocal microscopy gives blurry and ill-defined images (Fig. 44.10). Consequences of this increase in S/N ratio and dynamic range become even more evident on deep/thick or whole-organ imaging. In a quantitative comparison with confocal and widefield epi-fluorescence, TPE was recently shown to outperform the other methods in terms of effective resolution (Cox and Sheppard, 2004).

### Imaging Thick/Opaque Specimens

The second generally accepted TPE advantage is its capacity to image deep into tissues that usually allow poor or no penetration in confocal microscopy. This trend is well reflected in the literature and in our own studies on whole-organ imaging of *Arabidopsis* (Feijó and Moreno, 2004). However, it should be pointed out that the ability to image whole organs or thick tissues varies tremendously, especially in plants. Although people have been able to image  $>500\mu\text{m}$  into living brain (M. Vaz Afonso and T. Bonhoeffer, personal communication), brain tissue is far less opaque than most plant tissues. As a result, penetration values this large are very uncommon for botanical specimens unless they have first been fixed and cleared.

On some tissues, we could not penetrate through more than the epidermis (e.g., *Arabidopsis* living styles), apparently because it is covered with an outer cuticle that is so opaque that deeper penetration requires laser power levels that damage the tissue (they can literally boil the epidermal cells). Other tissues (e.g., immature anthers of *Agapanthus*) are reasonably transparent and allow live imaging up to the full working-distance of a high-resolution oil-immersion lens (ca.  $200\mu\text{m}$ ). Roots usually allow much deeper imaging than leaves or other green tissues [Fig. 44.10(A,B)]. Add a low level of stain to these absorption problems, with the frame averaging and the extra excitation/fading this implies, and one can see that any estimate on how deep one can go must be assessed on a case-by-case basis.

Several direct comparisons of confocal and TPE microscopy are offered in the literature. Vroom and colleagues (1999), working on microbial biofilms, made a quantitative comparison of signal intensity, and concluded that, compared to confocal, they were able to record images four times deeper and that these deep images did not lose contrast. In fixed material embedded in Nanoplast resin, TPE showed improvements both in penetration, contrast, and fade resistance (Decho and Kawaguchi, 1999). A practical example in which this improvement led to novel information was documented by Meyer and Fricker (2000). While studying glutathione distribution in different tissues, TPE provided more detail from optical sections deep in the tissue with less signal attenuation, and this ability was pivotal in being able to distinguish vacuoles from cytosol and to get a better separation of the sequestered signal.

On a more technical level, Sun and colleagues (2001) showed that the attenuation of the excitation signal in plant tissues is reduced with TPE. More significantly, Cheng and colleagues (2001b) made probably the most thorough analysis of signal attenuation as a function of the excitation wavelength (see Chapter 21, *this volume*). They determined that in mesophyll cells and whole leaf, while major attenuation of the signal occurs only below  $700\text{nm}$  (the major peak of attenuation at ca.  $690\text{nm}$ , attributable

to chlorophyll absorption), the attenuation decreases continuously up until about  $1000\text{nm}$ , which makes it clear that the longer the wavelength, the less appreciable will be the attenuation of the excitation signal.

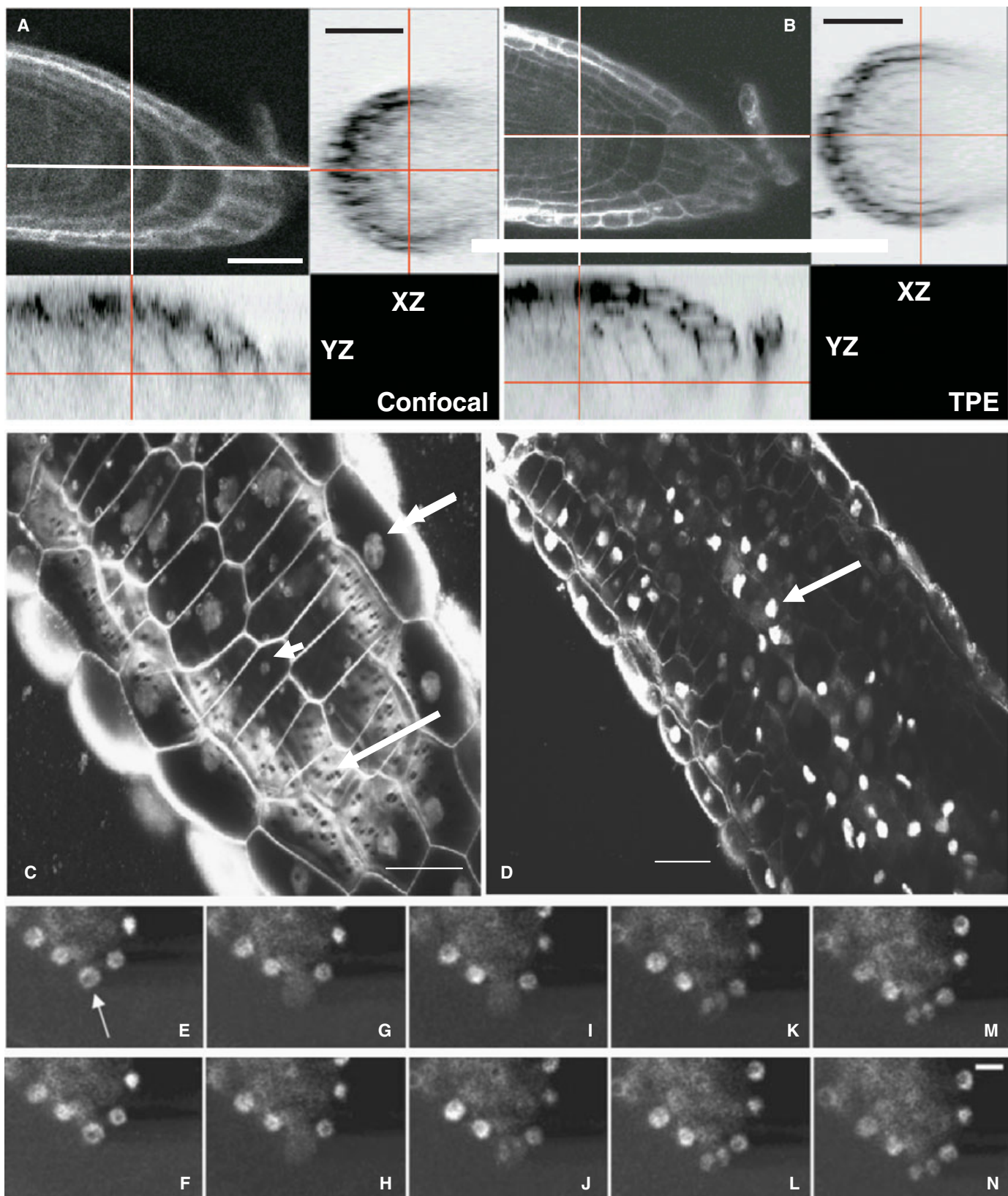
Better dynamic resolution and improved penetration are easy to demonstrate in a number of *Arabidopsis* organs. Figure 44.10 (A,B) show an application to whole, living roots, in which the cell walls have been stained with propidium iodide (PI) at a vital concentration. Comparison of Figure 44.10(A) (confocal) with Figure 44.10(B) (TPE) makes it clear: TPE provides high contrast and resolution to the mid-sagittal level of the root, in both  $yz$ - and  $xz$ -projections, and up to the 10th cell layer (the red lines indicate the relative position of the  $zz'$ -projections). This comparison is especially noteworthy as exactly the same specimen, optics, and acquisition protocol were used to obtain both images, and the only changes were the excitation source and the pinhole aperture (1 Airy unit for confocal and wide open for TPE). Because roots are cylindrical, this level of performance makes it reasonable to speak of the high-resolution characterization of an entire living root. In contrast, under the very same imaging conditions, confocal resolves no better than five cell layers (note that the red line indicating the projection plane is not even over the central stellar tissues), and the contrast and definition shown on the negative-contrast projection shows a clear deterioration of the signal as the image plane goes deeper.

In other organs, such as living leaves of *Arabidopsis*, penetration is much more limited (Feijó and Moreno, 2004). While one can appreciate improved dynamic range and better structural accuracy (specially with external, non-descanned PMTs), compared to confocal, TPE penetration was still barely more than  $50\mu\text{m}$  (see also Chapter 21, *this volume*). The conspicuous presence of abundant chloroplasts explains this result. Not only is penetration impaired, but specimen damage also becomes an issue. Complex interactions between all the pigments present can generate a number of potentially harmful products that may make TPE even more damaging than confocal in green tissues (see next section).

We have imaged living anthers at power levels consistent with structural recording of dynamic processes (Feijó and Cox, 2001). Both DNA stained with 4'-6-Diamidino-2-phenylindole (DAPI) and autofluorescence from the cell walls contribute to the observed fluorescence at  $780\text{nm}$  [Fig. 44.10(C,D)]. Under TPE, DAPI fades very little and produces a strong signal over an excitation bandwidth of more than  $100\text{nm}$  ( $720\text{--}850\text{nm}$ ). In confocal microscopy, the autofluorescence of the inner cell layers makes it difficult to image deeper than two to three cells, leaving the important *tapetum* and the sporogenic/meiotic cells occluded. However, under TPE, anthers show more transparency, allowing sections close to  $200\mu\text{m}$  [Fig. 44.10(B); 6–7 cell layers deep], which is the working distance limit of a high-NA immersion lens (in this case, a Nikon PlanApo,  $60\times$ , NA 1.4, oil). Remarkably, the same level of laser excitation was used to acquire the entire  $z$ -stack from the surface epidermis to the central sporogenic tissue [Fig. 44.10(A,B)]. With these improvements, an exquisite degree of contrast and detail is obtained in images of the pit fields and wall stress fibers in tangential/oblique optical sections of intermediary cell walls [Fig. 44.10(A), arrow]. The ability to image the mid-sagittal section of an anther allows direct viewing of the activities of meiotic cells (Feijó and Cox, 2001).

### Fading, Vital Imaging, and Cell Viability

Two-photon excitation is effectively confined to a sub-femtoliter volume at the point of focus within the sample, and although it is



generally agreed that TPE can minimize phototoxicity and fading during microscopy (Potter, 1996), a word of caution is due in many situations. As both damage and signal is proportional to (at least) the square of the power, power control is often a critical issue. Fragile tissues or those that dissipate heat poorly may pose a problem. For example, thin, fixed, sectioned materials (e.g., specimens used for immunolabeling) are sometimes much more difficult to image with two-photon than using widefield or confocal microscopy, because, in the focus plane, fading occurs more strongly with TPE. Clearly, TPE is not a cure-all.

It takes some effort to determine the best experimental conditions for vital TPE imaging, and it is particularly important to find the best balance between power, excitation wavelength, and probe concentration (when controllable). It usually implies a careful search for the best wavelength (one that maximizes S/N while minimizing photodamage) and then setting the power level so that there is just enough signal to form an image. The tuneability of titanium:sapphire (Ti:Sa) laser sources allows one to search for the optimum excitation wavelength, and this often leads to the choice of a wavelength away from the peak in the excitation spectrum. Continuous wave laser sources used for confocal microscopy are generally restricted to a small number of discrete excitation wavelengths, which makes this sort of optimization impossible. As a rule of thumb, the longer the wavelength the less the damage. Even at low power, using wavelengths less than 800 nm often causes much more damage in the form of fading, arrest of streaming or even slowing growth. A second rule of thumb is that wavelengths longer than 870 nm are almost always more suitable for imaging plant cells. Finally, dye molecules that are more asymmetrical (e.g., DAPI) tend to show better results than symmetrical ones [e.g., fluorescein isothiocyanate (FITC)]. In symmetrical molecules, usually more than one excitation peak is obtained, and using the longer wavelength tends to produce much better results in terms of less fading, even though it may also show less emission.

An exhaustive analysis and comparison of metabolic imaging led Fricker and Meyer (2001) to conclude that TPE might be the best means to study primary metabolism *in vivo*, if and when the relevant probes are produced and optimized. Because pollen tubes

show easily observable signs of vitality in the form of streaming and growth, we have used them to assay comparative phototoxicity. Being relatively resistant to radiation, they can also be used to studying fading (Feijó and Moreno, 2004). When viewing sensitive features such as actin dynamics, streaming, growth rate, pump activity, etc., TPE always seems to produce superior results when operated above 870 nm. For example, expression of an ADF:GFP construct that labels actin microfilaments in pollen tubes, combined with TPE allowed the collection of up to 600 sequential frames without interval, without producing noticeable fading, and with minimal effect on cell growth rates.

Figure 44.10(E–N) illustrates another example of a result difficult to achieve using confocal microscopy. Phil Benfey's laboratory produced lines of *Arabidopsis* with GFP (von Arnim *et al.*, 1998) fused to the putative transcription factor *Shortroot* (*SHR*) under the control of its own promoter and these were then imaged using TPE in our laboratory. Again, better contrast, dynamic range, penetration, and sensitivity were obtained, and the whole root was imaged down to the distal side of the central stele using TPE at 920 nm. Despite the weak signal, a diffuse cytosol labeling was discernable in the central stele cells and labeling in the nuclei of the endodermis shows a perfectly resolved and exclusive perinuclear location of *SHR*. Many of these features are not easily resolved in the equivalent confocal images. The TPE images helped to support the exciting finding that transcription factors may move between cell layers (Hake, 2001; Nakajima *et al.*, 2001), and *SHR* was assigned a role in defining cell fate in the root (Nakajima *et al.*, 2001). The sequence in Figure 44.10(E–N) shows frames of a division of a root meristematic cell (arrow), in which the putative transcription factor diffuses out during nuclear envelope breakdown and later re-aggregates in the two daughter nuclei. Using standard confocal, the signal faded before all the data could be collected because the extremely low fluorescence levels required a number of frames to be averaged to produce each high-definition optical section (G. Senna, 2002, personal communication). In the TPE results shown here, not only was fading reduced to a manageable level, but the radiation seems not to have affected either the division cycle or root growth to any measurable extent.

**FIGURE 44.10.** Imaging of a whole, living root of *Arabidopsis*, vitally stained with PI (10 µg/mL; wild-type root at ca. 8–12 days after germination) with confocal (A) and TPE (B) microscopy. In healthy cells, the membrane is impermeable to PI, rendering the cell wall fluorescent and clearly defining the cell boundaries. (A) The central confocal image shows an optical section 30 µm deep. The right and bottom panels show negative images of *xz* and *yz* reconstructions of the whole *zz*-stack acquired (confocal excitation using the three visible-light lines of the Kr: Ar-ion laser, emission filter HQ 598/40; the stack was acquired with 0.5 µm steps). The lines mark the relative position of the reconstructions on the central image, or the depth of the specific plane shown on the side panels. Wall boundaries, although visible, are diffuse, despite generous use of Kalman averaging. Three-dimensional projections accentuate that feature, and the *xz*-image shows little contrast and resolution beyond 4 to 5 cell layers. Thus, it is only possible to image the half-diameter of the whole root up to about 100 µm from the tip and the important context of the central stele is lost. Bar = 50 µm. Plan Fluo 40×, oil-immersion objective (NA 1.3) However, under TPE (B), anthers show more transparency, allowing sections close to 200 µm [Fig. 44.5(B); 6–7 cell layers deep], the working distance limit of a high-NA immersion lens. (Reproduced from Moreno and Feijó, 2004, with permission from Springer-Wien.) (C) Image of a living *Agapanthus umbelatus* anther, stained with DAPI. This organ is very translucent, permitting imaging up to the working-distance limit of a high-NA objective (ca. 200 µm, montage from surface to ca. 200 µm is shown from a to f). Nuclei (C, double arrow), cell walls (arrow), and plastids (arrowhead) all show some autofluorescence. (D) A tangential optical section through the cell wall of the third to the fourth cell layer reveals pit fields and cellulose stress directions with exquisite detail. Detailed nuclear structure is clearly visible up to the seventh cell layer, eventually reaching the central meiocyte tissue (B, arrow). Imaged with a Plan Apo 60×, oil-immersion objective (NA 1.4); excitation, 780 nm; no barrier emission filter, internal PMT. Bars: (C) 20 µm; (D) 50 µm. (Reproduced from Feijo and Cox, 2001, with permission from Elsevier.) (E–N) Time-lapse sequence of the division of a meristematic cell in the apex of a lateral root of *A. thaliana* that is expressing a fusion protein constructed of *SHR* and GFP. The montage was extracted from a sequence acquired with a rate of 1 frame/5 min over almost 3 h. During that period the root grew unaffected, and several meristematic and endodermal cells divided. In this sequence, a meristematic cell is shown throughout the cell cycle: the *SHR*:GFP fusion protein is first located at the periphery of the nucleus (E, arrow), but diffuses to the cytosol as soon as the nuclear membrane disappears (G). At this stage, the fluorescence seems continuous with the central stele cells (G–I). Following division and by the onset of cytokinesis (J–L) the nuclei are again discrete and *SHR*:GFP is again visible in the two daughter nuclei (K–N). (Excitation, 920 nm; emission, 530 nm; external PMT.) Bar = 10 µm. (Reproduced from Feijo and Moreno, 2004, with permission from Springer-Wien.)

Again, a word of caution should be issued. Potential pitfalls will remain until the right conditions to image specific probes in particular tissues are better defined. Until then, any study should be undertaken systematically, with time allowed for long sessions in which the procedures can be optimized for a particular experimental condition.

There are also cases where confocal provides the faster and more reliable path. In a recent case reported by Reddy and colleagues (2004), the shoot apical meristem (SAM) was imaged in an attempt to resolve a number of cell and organ-fate issues (Running, *et al.* 1995). A number of transgenic lines with markers of cell division and cell fate were created, and methods were developed for imaging the shoot growth on the same confocal plane for over a week. The workers were able to image deep stacks encompassing the whole meristem down to the first primordia every 4 h (Reddy *et al.*, 2004). Using Zeiss optics and confocal scanner, they made extensive comparisons with TPE and concluded that confocal significantly outperformed TPE in terms of keeping the SAM growing and dividing (Reddy, personal communication). Being a green tissue, these results come as no great surprise because, as we discussed in the autofluorescence section, the complex interaction between pigments and the high levels of near-infrared radiation makes it predictable that green tissues will always pose a problem for TPE imaging. This example should definitely be kept in mind when deciding on the amount of time and effort one might need to develop a viable protocol with a new method.

## Two-Photon Imaging of Plant Cells and Organelles

To date there is a growing body of literature showing the application to TPE of practically all of the common dyes and labels used for visible, one-photon fluorescence. Here we restrict ourselves to plant applications, plus our own experience managing a multi-user facility (see also Table II in Feijó and Moreno, 2004; Chapter 17, *this volume*). Again, most information regarding the use of different dyes with TPE should be considered preliminary and dependent on the specific experimental context (dye, vital/fixed samples, microscope, etc.). The available information should be used as a starting point for the process of fine tuning. Implicit in this statement is the recognition that it is difficult to obtain clear reproducible spectra for TPE excitation. In contrast to confocal microscopes and spectrofluorimeters, in which power can be kept within close tolerances and the average level has little variation, TPE depends critically on the peak power, which changes dramatically (i) along the tuning range of most ultrafast lasers, (ii) with position inside the focal volume, and even more so (iii) with the pulse width. Generally speaking, longer wavelengths provide shorter pulses, hence higher peak powers. To complicate matters, the average output power of a Ti:Sa laser peaks at around 800 nm, but falls off rapidly at the extremes of the tuning range. As most biology laboratories do not possess (or want to!) the very complex analytical instruments necessary to measure TPE cross-sections properly, wavelength-optimization routines are more likely to be based on somewhat crude empirical experiments. Data are often hard to reproduce directly on another system with different optics and design, but the experimental parameters are often close enough to indicate a range for optimization. One important reference that should be kept in mind is the classic work of Xu and Webb (1996) listing spectra for most of the commonly used dyes. [For updates, check the largest library of TPE spectra at [www.drbio.cornell.edu](http://www.drbio.cornell.edu); a small list of commonly used dyes is also given in Diaspro and Robello (2000).]

The ultraviolet (UV)-excited DNA dyes DAPI and Hoechst 33342 are TPE dyes *par excellence* and it is of no surprise that one or the other has been used in every paper published so far to illustrate the TPE principle (e.g., Denk *et al.*, 1990; König, 2000; Tirlapur and König, 2002). In plant tissues other than the classical onion root system, these dyes have been used to image live meiotic nuclei in anthers (Feijó and Cox, 2001), nuclear distribution during arbuscular mycorrhization of *Aspergillus nidans* and tomato (Bago *et al.*, 1999) and deep imaging in Nanoplast-embedded tissues (Decho and Kawaguchi, 1999). The popularity of these dyes is due to the fact that they are extremely bright and fade resistant under TPE, and that they can be excited over a wide range of wavelengths (720–850 nm for DAPI in our system), a feature that facilitates double- and triple-labeling as well as searches for the best vital imaging conditions.

TPE of Nile red has been used to follow the mobilization of lipid globules in fungal hyphae (Bago *et al.*, 2002). Autofluorescence was used for high-resolution dynamic analysis of chloroplast division (Tirlapur and König, 2001) and to study the cell wall (König, 2000).

Perhaps one of the most interesting and informative trends relates to TPE visualization of glutathione (GSH). The method was introduced to plants by Fricker and colleagues (2000), and it uses the dyes monochlorobimane (MCB) and monobromobimane (MBB), which complex with GSH to produce glutathione-S-bimane (GSB). Under normal confocal, these workers determined the concentration of GSH to be 2 to 3 mM in most cell types. However, using TPE, they were able to obtain more detail with less signal attenuation deep in the tissue and this was pivotal in distinguishing vacuoles from cytosol to get a better separation of the sequestered signal (Meyer and Fricker, 2000). Only under TPE was it possible to measure that GSH concentration in trichoblasts ( $2.7 \pm 0.5$  mM) was significantly different from that in atrichoblasts ( $5.5 \pm 0.8$  mM). More recently, trichomes were shown to have 300× more GSH than cells from the basement layer and the epidermis (Gutierrez-Alcalá *et al.*, 2000). These, and other results, support the conclusion that TPE is currently the best approach to studying primary metabolism *in vivo* (Fricker and Meyer, 2001; Meyer *et al.*, 2001).

## TPE Imaging of Green Fluorescent Protein

TPE is well suited for viewing GFP in plants (Xia *et al.*, 1999; Volkmer *et al.*, 2000), and indeed GFP is easily excitable at a wide range of wavelengths and in combination with other dyes, such as propidium iodide [Fig. 44.3(F)]. Special manipulation of the GFP levels have been used to raise signals above the wild-type chlorophyll autofluorescence by using “super” promoters, such as 35S35SAMV, driving especially bright GFPs, such as S65T, a combination successfully used to visualize mitochondria using TPE with good S/N even in green tissues (Köhler *et al.*, 1997). This example points to the need to consider the different kinds of GFP currently available.

The first one introduced was the wild-type GFP which, while excitable at about 800 nm, faded rapidly, perhaps even more so than with confocal. This and other problems led to the development of several enhanced forms of GFP. Here we offer data about some of the commonly-used forms: Clontech’s EGFP, Jim Haseloff’s mGFP forms (Siemering *et al.* 1996; Haseloff *et al.*, 1997) and also the forms engineered by Chiu and colleagues (1996) and by von Arnim and co-workers (1998).

Clontech’s version is perhaps currently the most popular. It shows a relatively broad TPE excitation peak from 920 to 940 nm, but can hardly be visualized below 900, unless under very strong

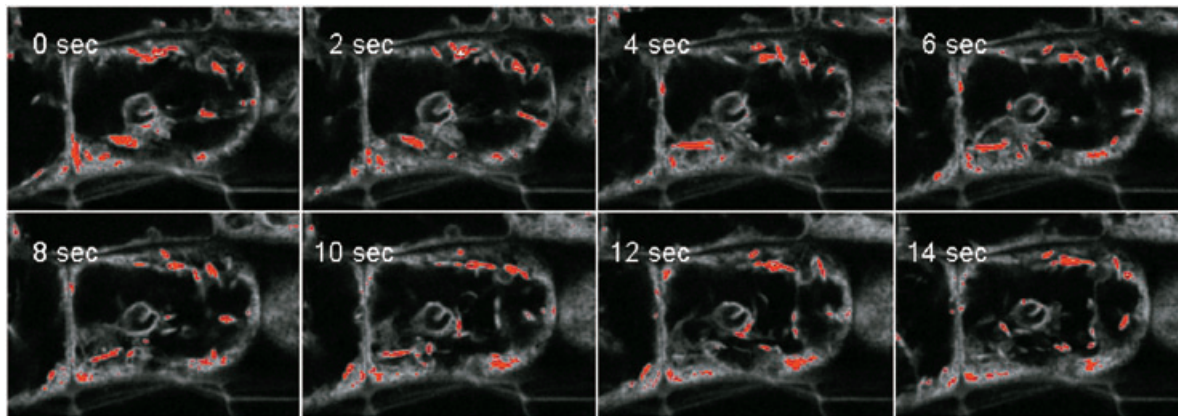


**FIGURE 44.11.** Fast dynamics in plant cells is illustrated by the movement of the protein inclusion on the ER of the hypocotyl epidermis on enhancer trap lines with GFP fused to an ER motif. In this specific sequence, TPE at 870nm was used to stretch the limits of viability of this kind of imaging. The images shown were extracted from a time series of a consecutive (no interval) sequence of acquisitions, which was extended up to 650 frames. Despite the amount of exposure, we observed no effect on fading or streaming rates.

promoters or when fused to abundant and stable proteins. Although these wavelengths are near the edge of the tuning range of the Ti:Sa laser and produce some dye fading, they still produce better images than with confocal microscopy [Fig. 44.3(B)], and even very faint markers such as membrane transporters can be imaged in living cells. The same result was obtained for the S65T mutation described by von Arnim and colleagues (1998) [Fig. 44.10(E–N)].

Nevertheless, we have found that the two other enhanced-GFP versions (Chiu *et al.*, 1996; Siemerling *et al.*, 1996) are even better for our purposes. First, they seem to behave best at 870 to 890 nm, a much more convenient wavelength range for the Ti:Sa laser, and one that any user can mode-lock. Second, if reasonably expressed, they seem to experience no quantifiable fading, even when sequentially imaged (Fig. 44.11). They provide high-resolution signals, and the mGFP5-ER, expressed in enhancer-trap lines, provides superb material for structural characterization, either alone [Fig. 44.3(D,E)] or in combination with PI [Fig. 44.3(F)]. Fine details of the nuclear envelope and of the ER-derived system are resolved, and the exclusive location of the tag in the endodermis is evident from the cell-edge fading that can be seen in tangential optical sections of the root. In streaming movements of the cortical ER, large particles have been followed in mGFP5-ER enhancer trap lines during many hundred consecutive frames, without any visible fading or quantifiable effect on the streaming rates and patterns (Hawes *et al.*, 2001; Fig. 44.11). These two engineered forms of GFP have proven to be exceptional tools for TPE in plants, and can be expected to become the source of many important advances in our understanding of dynamic cell and developmental processes.

## DYNAMIC IMAGING

While cell mobility in plants is strongly limited by the presence of a semi-rigid extracellular matrix, plant cells can display impressive spatial dynamics at the subcellular level. Generally speaking, cytoplasmic streaming is much faster than mechanical movements in animal cells, with organelles moving up to  $2\mu\text{m/s}$  [e.g., ER inclusions on *Arabidopsis* hypocotyl epidermis (Fig. 44.11) or mitochondria in pollen tubes [(Fig. 44.12)]. The easiest way to

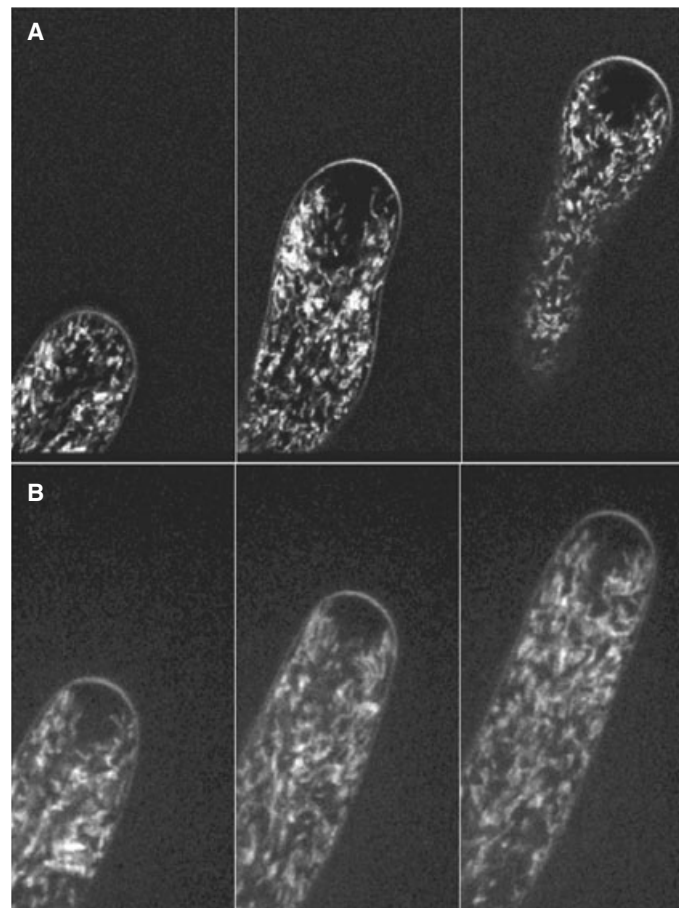


**FIGURE 44.12.** Comparison of spinning-disk and TPE imaging effects on pollen tube growth. Rhodamine 123-labeled mitochondria in *Lilium longiflorum* pollen tubes after 600 consecutive acquisitions. Frames were taken consecutively without any interval (1 frame/2 s) in the case of the TPE (820 nm excitation with an emission at 598/40 nm) at a speed of 5/s in a scanning disk (488 nm excitation with a triple dichroic). Unlike laser-scanning confocal (Feijó and Moreno, 2004), both systems show a very low phototoxicity. However, in the case of the TPE we should point out the low noise picture, and, in the case of the spinning-disk, the fast image acquisition. With TPE, the growth rate decreases by 30% compared to 10% with the NSDC.

image such a fast process is to use a widefield microscope with a scientific-grade charge-coupled device (CCD) camera, and apply a cost-effective algorithm to the two-dimensional (2D) data, such as no-neighbors 2D filtering (Monck *et al.*, 1992; McNally *et al.*, 1999). This method is similar to one developed by Castelmann (1979), in which three planes are acquired and the information of the outer planes subtracted to produce an improved image of structures present in the central plane.

However, more stringent applications do need optical sectioning. In many cases, deconvolution is not fast enough to provide enough temporal resolution on a moving sample, and other methods, such as single-beam laser-scanning microscope (LSM), TPE, or Nipkow spinning-disk confocal (NSDC), or even video-rate confocal (VRC) must be used.

Frame size is the next critical choice. In a LSM/TPE, one can go up to a few frames per second by choosing a box of only ~10 kilopixels, usually at the cost of proper sampling and, therefore, resolution. For many applications, as long as one does not need to go faster than 2 to 3 frames per second (fps), it is possible to find a compromise between speed and resolution. On the other hand, if speed and resolution are needed simultaneously, a different approach is needed.

NSDC and VRC use detectors that need time to integrate: thus, the dimmer the sample, the more time needed to record a decent picture. As most spinning-disk confocals use cooled CCD cameras [or the new intensified CCDs or even an electron multiplier (EM)-CCDs], one can adjust the exposure time and the binning independently. The first parameter affects acquisition speed and the second, resolution. Sensitivity is an issue, and exposures as long as several seconds are not unusual for lightly-stained specimens. Binning  $2 \times 2$  in a megapixel, cooled CCD improves this parameter dramatically. Although it will bring the effective pixel size close to the Nyquist sampling criteria, either the exposure time can be reduced to roughly one quarter or the S/N increased by a factor of 2.

Though common sense suggests that plant cells should be able to handle lots of light, this is not always true. Because their growth rate is quite sensitive to light, pollen tubes can be used to quantify phototoxicity. As previously mentioned, as long as a reasonable amount of signal is present, TPE above 870 nm produces almost no effects on the growth and streaming rates of pollen tubes [Fig. 44.12(A)]. However, even when imaging continuously, without interval, good resolution still implies a 2s frame-scan time. At this speed, much of the dynamics of fast-moving organelles, such as ER (Fig. 44.11) or especially, streaming mitochondria (Fig. 44.12) will be lost.

Provided that there is enough signal to allow use of a fast CCD (the case in Fig. 44.12, stained with the very bright Rhodamine 123), Nipkow-disk-based systems, such as the PerkinElmer/Yokogawa, definitely show a much more informative view [Fig. 44.12(B)]. In this case, it was easy to achieve an increase of one order of magnitude in the time resolution (2 s/frame on TPE and 200 ms/frame with the NSDC) and this allows one to clearly visualize different cytoplasmic domains in which mitochondria move faster or slower. We were unable to record similar data with any single-beam scanning method. As can be appreciated by comparing Figure 44.12(A,B), although the optical thickness is lower, the more accurate dynamic picture clearly outweighs the information lost by lower  $z$ -resolution. The ability to record a  $z$ -stack of a large, intact specimen in a fraction of the time also makes the technique suitable for time-lapse studies of fast-moving or growing organs.

We expect that NSDC microscopes will be crucial to being able to resolve fine temporal dynamics with minimal fading. The sensitivity issue does exist, and lightly-stained samples such as

many GFP-fusion lines could either not be imaged at all, or required an integration time so long that the system performance was less than that of TPE. Intensified CCDs or EM-CCDs may soon change this picture quite dramatically, and bring sensitivity to the level of TPE and LSM. Although the new generation of VRCs use high-speed computer interfaces with a bandwidth of 100 MB/s that permit high frame rates, problems with singlet-state saturation prevents single-beam confocal scanners from providing useful information about biological specimens except at low spatial resolution. On the other hand, high-speed line-scanners such as the Zeiss 5-Live avoid this trap by scanning many points at one time (see Chapter 10, *this volume*).

## DECONVOLUTION

In the last two decades there has been a boom in the use of 3D microscopy in biology, and botanical samples are no exception (Hepler and Gunning, 1998). Although this trend has been driven largely by the emergence of the confocal microscope, widefield microscopes can also generate raw 3D data, and software that can run on any modern personal computer is now available to extract sharp, 3D reconstructions from these data.

If one considers a microscope to be a “convolution machine,” its transfer function can be determined by measuring its response to a subresolution fluorescent bead: namely, its point spread function (PSF). To the extent that one knows the PSF and records the widefield 3D data stack accurately,<sup>1</sup> one should be able to invert the convolution process (deconvolution) to obtain a 3D image of the object imaged. The details of both convolution and deconvolution are covered in detail in Chapters 23, 24, and 25.

Because of the difficulties encountered when trying to measure the PSF, we usually make an average PSF from the 3D images of several beads (Holmes *et al.*, 1995). Although the biggest drawback of this approach is the requirement that the sample must not move or change during data acquisition (restricting the technique to fixed cells or structures moving very slowly), even minimal problems with the optics, such as misalignment, spherical aberration, and dirtiness, will affect the final image to a much greater extent than in confocal and TPE. To some degree, it may be possible to compensate for the degradation of the PSF brought about by spherical aberration (Boutet de Monvel *et al.*, 2001) or by the heterogeneous refraction index of a living cell (Kam *et al.*, 1998). As these techniques improve, they may be important when deconvolution techniques are applied to images of plant cells in which, for example, spheroidal central vacuoles can act as miniature lenses. Despite these limitations, deconvolution retains some substantial advantages for living-cell microscopy: phototoxicity, photobleaching, and price are all often lower.

It is also important to note that **deconvolution protocols not only can, but should, be applied to all 3D confocal and TPE data sets**. Doing so not only substantially reduces the “single-pixel noise features” produced by the statistical uncertainty attendant on measuring small numbers of photons, but it also substantially improves the statistical accuracy of the image data by effectively averaging the signal over many voxels (see Chapter 25, *this volume*).

<sup>1</sup> The main practical limitation to doing this is the presence of both Poisson and read noise in the final data.

**FIGURE 44.13.** The effect of deconvolution on a widefield stack. (A) A plane from a stack of a unicellular green algae. (B) A deconvolved version of the same plane using a measured PSF and a glycerol immersion objective (PlanApo 63× NA 1.3). The whole projection was about 30 μm deep (autofluorescence). The improvement in contrast is obvious, and is highlighted in the line scan. The PSF was generated using orange beads from Molecular probes (PS-Speck) with 170 nm diameter.

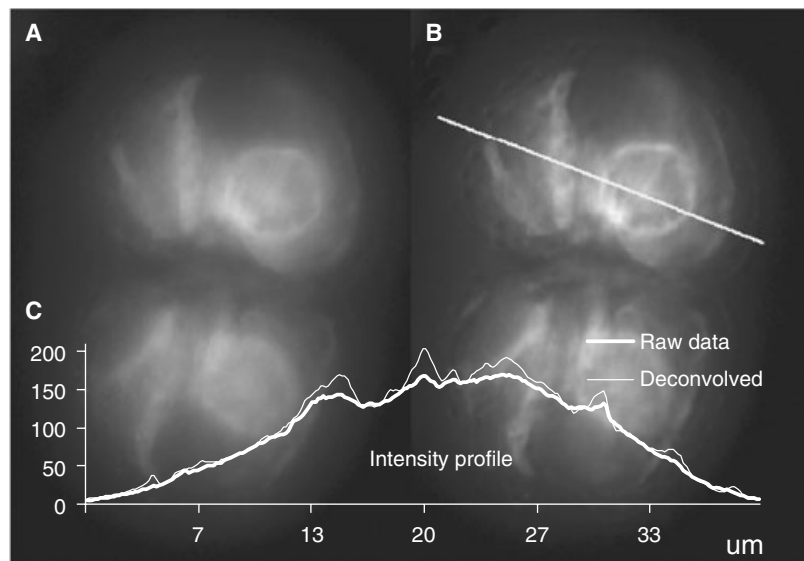


Figure 44.13(A) shows an autofluorescence image of a unicellular green alga. In this specific sample, several attempts with both confocal and multi-photon microscopes failed to produce a sharp image over extended focus stacks of the entire depth of the cell. The main problem was that the high intensity illumination caused the signal to get dimmer and the autofluorescence to shift from red to green (Cheng *et al.*, 2001). Deconvolution of data stacks collected using a much lower intensity of excitation light made a considerable improvement [Fig. 44.13(B)].

## CONCLUSION

Ever since the time of Hooke, plant cells have been the foundation of many of the fundamental discoveries that have shaped cell biology. Underlying all these findings were significant advances in microscopy that helped to push forward our conceptual thinking, for example, supporting the acceptance of the cell theory. In this chapter we have highlighted what is now the leading edge of this technological effort.

Imaging is now more than lenses and microscopes. Computers are also essential, both to accumulate and display research images, and to extract and analyse enormous amounts of quantitative information from them.

Recent advances range from major hardware (e.g., two-photon equipment) to the development of computer software that now enables us to derive fresh insights from old histological techniques.

We have tried to emphasize that all these techniques are only of value when they enable us to describe previously unknown biological features, and indeed many of the most important technical developments were developed only as part of specific research projects.

The ever-growing field of genetically-encoded probes, such as GFP, seems likely to trigger more new and important technical adaptations that will enable us to obtain more and better dynamic information from living systems. Plant cell biology continues to bloom, and much of this growth is supported by modern imaging methods.

## ACKNOWLEDGMENTS

The JAF laboratory is supported by FCT grants POCTI/BCI/46453/2002, POCTI/BIA-BCM/60046/2004, and POCTI/BIA-BCM/61270/2004. Some GFP lines from the Haseloff laboratory were imaged during the 2nd and 3rd Gulbenkian Biology Course on Plant Development (Oeiras, Portugal, 2003) by groups involving the students Niko Geldner, Vaiva Kazanaviciute, Jirina Prochazkova, Kasia Olczak, Martha Alvarado (a very special thanks for the MAP4 and talin lines), Lisa Gao, Martin Potocky, and Chris Nichols. The SB laboratory is supported by grants from BBSRC.

## REFERENCES

- Bago, B., Zipfel, W., Williams, R.M., Cahmberland, J.G., Lafontaine, J.G., Webb, W.W., and Piche, Y., 1998, *In vivo* studies on the nuclear behavior of the arbuscular mycorrhizal fungus *Gigaspora rosea* grown under axenic conditions, *Protoplasma* 203:1–15
- Bago, B., Zipfel, W., Williams, R.M., Jun, J., Arreola, R., Lammers, P.J., Pfeffer, P.E., and Shachar-Hill, Y. 2002, Translocation and utilization of fungal storage lipids in the arbuscular mycorrhizal symbiosis, *Plant Physiol.* 128:108–124
- Bago, B., Zipfel, W., Williams, R.M., and Piche, Y., 1999, Nuclei of symbiotic arbuscular mycorrhizal fungi as revealed by *in vivo* two-photon microscopy, *Protoplasma* 209:77–89.
- Blancaflor, E.B., and Gilroy, S., 2000, Plant cell biology in the new millennium: New tools and new insights, *Am. J. Botany* 87:1547–1560.
- Bolte, S., Talbot, C., Boutte, Y., Catrice O., Read, N., and Satiat-Jeunemaitre, B., 2004, FM-dyes as experimental probes for dissecting vesicle trafficking in living plant cells, *J. Microsc.* 214:159–173.
- Bougourd, S., Marrison, J., and Haseloff, J., 2000, Technical advance: an aniline blue staining procedure for confocal microscopy and 3D imaging of normal and perturbed cellular phenotypes in mature *Arabidopsis* embryos, *Plant J.* 24:543–550.
- Boutet de Monvel, J., Le Calvez, S., and Ulfendahl, M., 2001, Image restoration for confocal microscopy: Improving the limits of deconvolution, with application to the visualization of the mammalian hearing organ, *Biophys. J.* 80:2455–2470.

- Brandizzi, F., Fricker, M., and Hawes, C., 2002, A greener world: The revolution in plant bio-imaging, *Nat. Rev. Mol. Cell Biol.* 3:520–530.
- Castleman, K.R., 1979, *Digital Imaging Processing*, Prentice Hall, Englewood Cliffs, New Jersey.
- Chen, C.Y., Cheung, A.Y., and Wu, H.M., 2003, Actin-depolymerizing factor mediates Rac/Rop GTPase-regulated pollen tube growth, *Plant Cell* 15:237–249.
- Cheng, P.-C., Lin, B.-L., Kao, F.-J., Gu, M., Xu, M.-G., Gan, X., Huang, M.-K., and Wang, Y.-S., 2001a, Multi-photon fluorescence microscopy — The response of plant cells to high intensity illumination, *Micron* 32:661–670.
- Cheng, P.C., Sun, C.K., Lin, B.L., Kao, F.J., and Chu, S.W., 2001b, Nonlinear multimodality spectromicroscopy: Multiphoton fluorescence, SHG and THG of biological specimen, *Proc. SPIE* 4262:98–103.
- Chiu, W.-L., Niwa, Y., Zeng, W., Hirano, T., Kobayashi, H., and Sheen, J., 1996, Engineered GFP as a vital reporter in plants, *Curr. Biol.* 6:325–330.
- Chu, S.W., Chen, I.-H., Liu, T.-M., Sun, C.-K., Lee, S.-P., Lin, B.-L., Cheng, P.-C., Kuo, M.-X., Lin, D.-J., and Liu, H.-L., 2002, Nonlinear bio-photonics crystal effects revealed with multimodal nonlinear microscopy, *J. Microsc.* 208:190–200.
- Cox, G., & Sheppard, C., 2004, Practical limits of resolution in confocal and nonlinear microscopy, *Microsc. Res. Tech.* 62:18–22.
- Cutler, S.R., Ehrhardt, D.W., Griffiths, J.S., and Somerville, C.R., 2000, Random GFP::cDNA fusions enable visualization of subcellular structures in cells of *Arabidopsis* at a high frequency, *Proc. Natl. Acad. Sci. USA* 97:3718–3723.
- Decho, A.W., and Kawaguchi, T., 1999, Confocal imaging of in situ natural microfibril communities and extracellular polymeric secretions using nanoplast resin, *Biotechniques* 27:1246–1252.
- Denk, W., Strickler, J.H., and Webb, W.W., 1990, Two-photon laser scanning fluorescence microscopy, *Science* 248:73–76.
- Diaspro, A., and Robello, M., 2000, Two-photon excitation of fluorescence for three-dimensional optical imaging of biological structures, *J. Photochem. Photobiol. B* 55:1–8.
- Esau, K., 1977a, *Anatomy of Seed Plants*, John Wiley and Sons, New York.
- Esau, K., 1977b, *Plant Anatomy*, 2nd ed., John Wiley and Sons, New York.
- Fahn, A., 1990, *Plant Anatomy*, 4th ed., Pergamon, London.
- Feijó, J.A., and Cox, G., 2001, Visualization of meiotic events in intact living anthers by means of two-photon microscopy, *Micron* 32:679–684.
- Feijó, J.A., and Moreno, N., 2004, Imaging plant cells by two-photon excitation, *Protoplasma* 223:1–23.
- Fricker, M., Parsons, A., Tlalka, M., Blancaflor, E., Gilroy, S., Meyer, A., and Plieth, C., 2001, Fluorescent probes for living plant cells, In: *Plant Cell Biology, A Practical Approach* (C. Hawes and B. Satiat-Jeuemaitre, eds.), Oxford University Press, Oxford, United Kingdom, pp. 35–83.
- Fricker, M.D., and Meyer, A.J., 2001, Confocal imaging of metabolism *in vivo*: Pitfalls and possibilities, *J. Exp. Botany* 52:631–640.
- Fricker, M.D., May, M., Meyer, A.J., Sheard, J., and White, N.S., 2000, Measurement of glutathione levels in intact roots of *Arabidopsis*, *J. Microsc.* 198:162–173.
- Galbraith, D.W., Bohnert, H.J., and Bourque, D.P., eds., 1995, *Methods in Cell Biology*, Academic Press, New York.
- Galway, M.E., Heckman, J.W. Jr., Hyde, G.J., and Fowke, L.C., 1995, Advances in high-pressure and plunge-freeze fixation, In: *Methods in Plant Cell Biology* (D.W. Galbraith, H.J. Bohnert, and D.P. Bourque, eds.), Academic Press, New York, pp. 4–20.
- Grew, N., 1673, An idea of a phythological history propounded. Together with a continuation of the anatomy of vegetables, particularly prosecuted upon roots. With an account of the vegetation of roots grounded chiefly thereupon. Published by Nehemiah Grew.
- Gunning, B., 2002, Plant cell biology on CD, Author edition, www.plantcellbiologyoncd.com.
- Gunning, B.S., and Steer, M.W., 1996, *Plant Cell Biology: Structure and Function*, Jones and Bartlett Publishers, Boston.
- Gutiérrez-Alcalá, G., Gotor, C., Meyer, A.J., Fricker, M., Vega, J.M., and Romero, L.C., 2000, Glutathione biosynthesis in *Arabidopsis* trichome cells, *Proc. Natl. Acad. Sci. USA* 97:11108–11113.
- Hake, S., 2001, Mobile proteins signals cell fate, *Nature* 413:261–263.
- Haseloff, J., 1999a, GFP variants for multispectral imaging of living cells, *Methods Cell Biol.*, 58:139–151.
- Haseloff, J., 1999b, Imaging green fluorescent protein in transgenic plants, In: *Imaging Living Cell* (R. Rizzuto and C. Fasolato, eds.), Springer-Verlag, Berlin, pp. 40–94.
- Haseloff, J., 2003, Old botanical techniques for new microscopes, *Biotechniques* 34:1174–1178.
- Haseloff, J., and Amos, B., 1995, GFP in plants, *Trends Genet.* 11:328–329.
- Haseloff, J., Siemering, K.R., Prasher, D.C., and Hodge, S., 1997, Removal of a cryptic intron and subcellular localization of green fluorescent protein are required to mark transgenic *Arabidopsis* plants brightly, *Proc. Natl. Acad. Sci. USA* 94:2122–2127.
- Hawes, C., and Satiat-Jeuemaitre, B., eds., 2001, *Plant Cell Biology, A Practical Approach*, Oxford University Press, Oxford, United Kingdom.
- Hepler, P.K., and Gunning, B.E.S., 1998, Confocal fluorescence microscopy of living cells, *Protoplasma* 201:121–157.
- Holmes, T.J., Bhattacharyya, S., Cooper, J.A., Hanzel, D., Krishnamurthi, V., Lin, W., Roysam, B., Szarowski, D., and Turner, J., 1995, Light microscopic images reconstructed by maximum likelihood deconvolution, In: *Handbook of Biological Confocal Microscopy* (J.B. Pawley, ed.), Plenum Press, New York, pp. 389–402.
- Kam, Z., Hanser, B., Gustafsson, M.G.L., Agard, D.A., and Sedat, J.W., 2001, Computational adaptive optics for live three-dimensional biological imaging, *Proc. Natl. Acad. Sci. USA* 98:3790–3795.
- Ketelaar, T., Anthony, R.G., and Hussey, P.J., 2004, Green fluorescent protein-mTalin causes defects in actin organization and cell expansion in *Arabidopsis* and inhibits actin de-polymerizing factor's actin depolymerizing activity *in vitro*, *Plant Physiol.* 136:3990–3998.
- Kodama, H., and Komamine, A., 1995, Synchronization of cell cultures of higher plants, In: *Methods in Plant Cell Biology* (D.W. Galbraith, H.J. Bohnert, and D.P. Bourque, eds.), Academic Press, New York, pp. 315–330.
- Köhler, R.H., Zipfel, W.R., Webb, W.W., and Hanson, M.R., 1997, The green fluorescent protein as a marker to visualize plant mitochondria *in vivo*, *Plant J.* 11:613–621.
- König, K., 2000, Multiphoton microscopy in life sciences, *J. Microsc.* 200:83–104.
- Lloyd, C.W., 1987, The plant cytoskeleton: The impact of fluorescence microscopy, *Annu. Rev. Plant Physiol.* 38:119–139.
- Malkin, R., and Niyogi, K., 2001, Photosynthesis, In: *Biochemistry & Molecular Biology of Plants* (B.B. Buchanan, W. Gruissem, and R.L. Jones, eds.), American Society of Plant Biologists, New York, pp. 568–628.
- Mason, W.T., 1993, *Fluorescent and Luminescent Probes for Biological Activity*, Academic Press, London.
- McInerney, T., and Terzopoulos, D., 1996, Deformable models in medical image analysis: a survey, *Med. Image Anal.* 2:91–108.
- McNally, J.G., Karpova, T., Cooper, J., and Conchello, J.A., 1999, Three-dimensional imaging by deconvolution, *Microsc. Methods* 19:373–385.
- Meyer, A.J., and Fricker, M.D., 2000, Direct measurement of glutathione in epidermal cells of intact *Arabidopsis* roots by two-photon laser scanning microscopy, *J. Microsc.* 198:174–181.
- Meyer, A.J., May, M.J., and Fricker, M., 2001, Quantitative *in vivo* measurement of glutathione in *Arabidopsis* cells, *Plant J.* 27:67–78.
- Monck, J.R., Oberhauser, A.F., Keating, T.J., and Fernandez, J.M., 1992, Thin-section ratiometric Ca<sup>2+</sup> images obtained by optical sectioning of fura-2 loaded mast cells, *J. Cell Biol.* 116:745–759.
- Nakajima, K., Sena, G., Nawy, T., and Benfey, P.N., 2001, Intracellular movement of the putative transcription factor SHR in root patterning, *Nature* 413:307–311.
- Parthasarathy, M.V., 1995, Freeze-substitution, In: *Methods in Plant Cell Biology* (D.W. Galbraith, H.J. Bohnert, and D.P. Bourque, eds.), Academic Press, New York, pp. 57–70.
- Potter, S., 1996, Vital imaging: Two photons are better than one, *Curr. Biol.* 6:1595–1598.
- Raghavan, V., 1995, Manipulation of pollen grains for gametophytic and sporophytic types of growth, In: *Methods in Plant Cell Biology* (D.W. Galbraith, H.J. Bohnert, and D.P. Bourque, eds.), Academic Press, New York, pp. 367–377.
- Reddy, G.V., Heisler, M.G., Ehrhardt, D.W., and Meyerowitz, E.M., 2004, Real-time lineage analysis reveals oriented cell divisions associated with morphogenesis at the shoot apex of *Arabidopsis thaliana*, *Development* 131:4225–4237.

- Ruzin, S.E., 1999, *Plant Microtechnique and Microscopy*, Oxford University Press, Oxford.
- Running, M.P., Clark, S.E., and Meyerowitz, E.M., 1995, Confocal microscopy of the shoot apex, In: *Methods in Plant Cell Biology* (D.W. Galbraith, H.J. Bohnert, and D.P. Bourque, eds.), Academic Press, New York, pp. 217–230.
- Shav-Tal, Y., Singer, R.H., and Darzacq, X., 2004, Imaging gene expression in single living cells, *Nat. Rev. Mol. Cell Biol.* 5:856–862.
- Shaw, P.J., 2001, Introduction to optical microscopy for plant cell biology, In: *Plant Cell Biology, A Practical Approach* (C. Hawes and B. Satait-Jeunemaitre, eds.), Oxford University Press, Oxford, United Kingdom, pp. 1–33.
- Shaw, S.L., Kamyar, R., and Ehrhardt, D.W., 2003, Sustained microtubule treadmilling in *Arabidopsis* cortical arrays, *Science* 300:1715–1718.
- Sheen, J., 1995, Methods for mesophyll and bundle sheath cell separation, In: *Methods in Plant Cell Biology* (D.W. Galbraith, H.J. Bohnert, and D.P. Bourque, eds.), Academic Press, New York, pp. 305–314.
- Shimmen, T., and Yokota, E., 2004, Cytoplasmic streaming in plants, *Curr. Biol.* 16:68–72.
- Siemering, K.R., Golbik, R., Sever, R., and Haselhoff, J., 1996, Mutations that suppress the thermosensitivity of green fluorescent protein, *Curr. Biol.* 6:1653–1663.
- Spence, J., 2001, Plant histology, In: *Plant Cell Biology, A Practical Approach* (C. Hawes and B. Satait-Jeunemaitre, eds.), Oxford University Press, Oxford, United Kingdom, pp.189–206.
- Sun, C.-K., Chu, S.-W., Chen, I.-S., Liu, T.-M., Cheng, P.-C., and Lin, B.-L., 2001, Multi-modality nonlinear microscopy, *Conf. Lasers Electro Opt. Eur. Tech. Dig.* 2001:222–227.
- Tirlapur, U., and König, K., 2001, Femtosecond near-infrared lasers as a novel tool for non-invasive real-time high-resolution time-lapse imaging of chloroplast division in living bundle sheath cells of *Arabidopsis*, *Planta* 214:1–10.
- Tirlapur, U., and König, K., 2002, Two-photon near-infrared femtosecond laser scanning microscopy in plant biology, In: *Confocal and Two-Photon Microscopy: Foundations, Applications and Advances* (A. Diaspro, ed.), Wiley-Liss, New York, pp. 449–468.
- Volkmer, A., Subramaniam, V., Birch, D.J.S., and Jovin, T.M., 2000, One and two-photon excited fluorescence lifetimes and anisotropy decays of GFPs, *Biophys. J.* 78:1859–1898.
- von Arnim, A.G., Deng, X.M., and Stacey, M.G., 1998, Cloning vectors for the expression of green fluorescent protein fusion proteins in transgenic plants, *Gene* 221:35–43.
- Vroom, J.M., de Grauw, K.J., Gerritsen, H.C., Bradshaw, D.J., Marsh, P.D., Watson, J.J., Birmingham, C., and Allison, C., 1999, Depth penetration and detection of pH gradients in biofilms by two-photon excitation microscopy, *Appl. Environ. Microbiol.* 65:3502–3511.
- Wysocka-Diller, J.W., Helariutta, Y., Fukaki, H., Malamy, J.E., and Benfey, P.N., 2000, Molecular analysis of SCARECROW function reveals a radial patterning mechanism common to root and shoot, *Development*, 127:595–603.
- Xia, A.D., Wada, S., Tashiro, H., and Wang, W.H., 1999, One and two-photon fluorescence from recombinant GFP, *Arch. Biochem. Biophys.* 372:280–284.
- Xu, C., and Webb, W., 1996, Measurement of two-photon excitation cross sections of molecular fluorophores with data from 690 to 1050 nm, *J. Opt. Soc. Am. B* 13:481–491.